Short Title

A SPHERICAL HARMONIC ANALYSIS OF THE GLOBAL 1000 mb SURFACE

A SPHERICAL HARMONIC ANALYSIS OF THE GLOBAL 1000 mb SURFACE FOR SEPTEMBER 1957

by
Jacob Padro

A thesis submitted to the Faculty of Graduate Studies and Research in partial fulfillment of the requirement for the degree of Master of Science.

Department of Meteorology
McGill University
Montreal

April 1966

ABSTRACT

Characteristic features of the long atmospheric waves are discussed on the basis of spherical harmonic analysis of global weather charts for September 1957. At first, there is a discussion of the Trapezoidal and Simpson's numerical integration rules as applied to the computation of the Spherical harmonic coefficients. Then, there is a variance analysis of the waves with indices $1 \leq m \leq n \leq 15$; this includes a discussion of the quasi-stationary and travelling modes of some of the waves. In the last section, there is a description of the behaviour of some of the tesseral and zonal harmonics with regard to daily variance fluctuations, mean positions of the waves and vertical slopes.

ACKNOWLEDGEMENTS

It is a pleasure to acknowledge the assistance, encouragement and advice of my supervisor, Professor B.W. Boville, at all stages in the realization of this project.

Acknowledgement is made to Mr. P. Merilees for his assistance with the writing of the computer programs and stimulating discussions; to Mr. J.D. Henderson, and my wife for their help in extracting data and punching computer cards; to Mr. J. De Las Alas for draughting some of the diagrams and to Miss A. Chin-A-Loy for preparing the typescript.

The author is also grateful to the staff and his fellow graduate students in meteorology for their generous help in friendly discussions; to the staff of the McGill Computing Centre for the use of their facilities; and to the Meteorological Branch of the Department of Transport for financial assistance.

TABLE OF CONTENTS

LIST OF SYMBOLS

g	Gravitational acceleration
R_d	Gas constant for dry air
t	Time coordinate
θ	Colatitude angle
λ	Longitude angle
m	Order (rank) of a spherical harmonic
n	Degree of a spherical harmonic
T_v	Virtual temperature
P_c	1000 mb pressure
$P(\theta, \lambda)$	Surface pressure at a grid point (θ, λ)
$Z(\theta, \lambda)$	Height of 1000 mb surface at (θ, λ)
$\overline{Z}$	Area weighted mean of the height field
$Z'(\theta, \lambda)$	$Zi - \overline{Z}$
P_n^m	Normalized associated Legendre polynomial of (m, n)
A_n^m, B_n^m	Spherical harmonic coefficients
$A^m(\theta)$, $B^m(\theta)$	Fourier coefficients
C_n^m	Amplitude
ϕ_n^m	Phase angle
σ^2	Variance
μ_k	Zeros of P_k^o (high degree polynomial)
η_i	Latitudes at which $A^m(\theta)$, $B^m(\theta)$ are known
w	Weighting function for numerical integration
V	Velocity of the zonal circulation
α	Angular velocity of the air motion relative to the earth
v, u	Components of the perturbation velocity toward S, E.
ζ	Vorticity relative to the earth
a	Radius of the earth
ψ	Stream function

LIST OF FIGURES

Fig. | Page

INTRODUCTION

The atmospheric motion as it presents itself on global weather charts can be considered as a mean flow upon which are superimposed more or less marked disturbances. The disturbances however represent again a superposition of components with horizontal scales in a very wide range. Since surface spherical harmonics are characteristic functions of the non-linear vorticity equation, it seems appropriate to use them in the representation of the horizontal flow patterns. This type of analysis was applied to geomagnetic variables long before its introduction into meteorology by Haurwitz in 1940. Since then more work on spherical harmonics has been done by various people. This strengthened further the case for the use of these functions both on theoretical and practical grounds. However, the principal difficulty that stands in the way of a completely fruitful use of these functions is the lack of adequate data distributed over the whole earth.

The International Geophysical Year (1957-1958) provides data which covers much more extensive area than usual. This makes it possible to express the global height field in terms of spherical harmonics and obtain more meaningful results. As an indication of this, Figure 1b) shows the 1000 mb weather map of September 1st 1957 for the northern hemisphere, as represented by spherical harmonics. It is in very good agree-

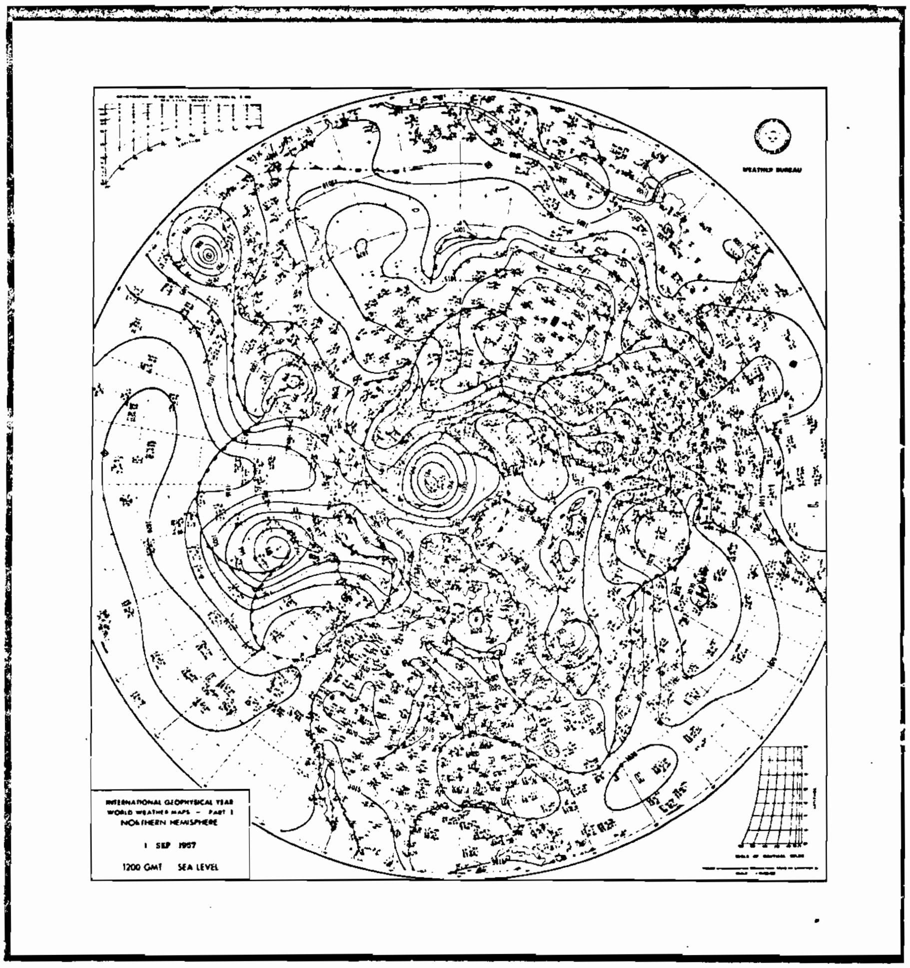

Figure 1a. Analyzed surface chart for September 1, 1957.

Figure 1b. Height distribution at the 1000 mb level for September 1, 1957 as represented by spherical harmonic analysis. The analysis contains the terms for which $0 \leq m \leq n \leq 15$.

ment with the actual surface map of Figure 1a). To facilitate comparison of the two maps, a geographical location will be denoted by (θ λ) in the following description. The centres of the lows at (55°, 160° W), (50°, 147.5° E) in the computed map coincide with the two respective lows on the actual map, but the low near the pole is about 7° west of the actual map's low. The low pressure areas at (60°, 20° E) and (50°, 60° W) and the Highs at (55°, 65° E) and (40°, 55° W) of the computed map coincide respectively with those of the actual map. It is not worthwhile to compare the more southern systems because of the poor analysis of the actual map near the boundary.

Background

Early pioneers in the work of spectral models for the atmosphere are Rossby (1939) and Haurwitz (1940). Rossby has given a simple theory relating the dimensions and velocities of perturbations with the zonal component of the general atmospheric circulation. He assumes that the lateral extent of these centres, i.e., their width, in meridional direction, is infinite and furthermore that the earth may be regarded as flat. Haurwitz extended the idea to include the sphericity of the earth and gave the perturbations a finite lateral extent.

Haurwitz and Craig (1952) made a study of the 3 km pressure field between 20N and 60N by spherical harmonics for the period January 1st to January 9th 1938. Lack of data limited their analysis to this latitude belt. Only terms with m=1, 2, 3, 4 and n=m+1, m+2, m+3, were used. Their results gave far too intense and fast-moving systems. This is somewhat expected since the theory applies well to the whole globe rather than to a limited latitudinal belt.

J. Namias and K. Smith (1943) also analyzed by spherical harmonics the 3 km normal pressure fields for January, April, July and October. The analyses were conducted for data between 20N and 60N. They found that in April and October, the terms with $m=3$ become of relatively greater significance. The behaviour of the phase constant was rather disquieting. This seems to indicate that the harmonic analysis applied to data of a limited area is nothing but a formal result without much physical significance.

In a recent study by Eliasen and Machenhauer (1965), the analysis was done over the northern hemisphere using even waves to represent the height field and odd waves to represent the stream function field. Both the 1000 mb and the 500 mb surfaces were analyzed for the 90 day period from December 1, 1956 to February 28, 1957. They find the amplitude to be growing with height except for the component $(m, n)=(1, 4)$. Comparing their values from the two levels, it is seen that for all components with $m \leq 3$ and $n \leq m=5$, the position at 500 mb level is to the west of the position at 1000 mb level, the distance being about 0.2 times the wavelength.

There seems to be so far only one study of the global height field by surface spherical harmonics. These functions were applied to 500 mb height field by Steinberg for the month of September 1957. He suggests that components with $m=1$ behave in the same manner in both hemispheres, i.e., they are mainly quasi-stationary and have large values of variance, while components with $m=4$ propagate eastward with relative phase velocities in both hemispheres. Also, for this order of the wave $(m=4)$, the variances of the odd component seem to be out of phase with those of the even components, a fact which leads him to the conclusion that there was energy transfer between some of the odd and some of the even components.

Data Sources

Surface pressure data over the globe were extracted from maps issued by an I.G.Y. Special Committee. Three nations were involved in the analysis of these maps, namely the Federal Republic of Germany, Republic of South Africa and the United States of America. U.S.A. handled Part I (Northern Hemisphere, 20N to the pole), F.R.G., Part II (25S to 25N), and R.S.A., Part III (Southern Hemisphere, 20S to the pole).

The I.G.Y. World Weather Maps consist of a daily series of maps for the period July 1, 1957 to December 31, 1958. These maps are published as monthly booklets, each containing a surface and 500 mb maps for 1200 GMT each day. Each hemispheric chart (Parts I, II) is a polar stereographic projection from 20 degrees to the pole with the true scale of 1 to 50 million at latitude 60 degrees. Part II is a mercator projection, with true scale of 1 to 50 million at latitude $22\frac{1}{2}$ degrees.

Temperature data were extracted from the Monthly Climatic Data for the World, sponsored by the World Meteorological Organization in cooperation with the U.S. Weather Bureau.

Data Extraction

The spherical harmonic series for each one of the 30 maps contains amplitude for 136 components and phase angles for 120 components. These were obtained from height data of the 1000 mb surface at a network of 1262 points (intersections of meridians divisible by 10 and parallels of latitude divisible by 5). The height data were calculated from surface pressure data at each grid point and the mean monthly temperature for each latitude.

Angles of colatitude were measured from $\theta=0$ degrees at the north pole to $\theta=180$ degrees at the south pole. Angles of longitude were measured from Greenwich meridian and eastward. The cards were processed through McGill's IBM 7044, 32000-word digital computer.

THEORY

Height Computation

The 1000 mb heights were calculated through the Hypsometric Equation,

$$Z(\theta,\lambda) = \left(\frac{R_d}{g}\right) \overline{T}(\theta) \ln \frac{P(\theta,\lambda)}{P_c}$$

where,

R_d = 287 joules kg^{-1} ^{o}k, gas constant for dry air

g = 9.80665 m-sec^{-2}, gravitational acceleration

$\overline{T}$ is the mean virtual temperature between the surface and the 1000 mb pressure levels. Measured in degrees Kelvin, the mean monthly surface temperature as a function of latitude (or colatitude) is found sufficiently accurate.

$P(\theta,\lambda)$ is the surface pressure at (θ,λ) in mb

P_c is the constant pressure of 1000 mb

Z is the height of the 1000 mb level at (θ,λ) in decameters

Spherical Harmonic Representation of the Height Field

As a basic material, the present study uses the height of a surface of constant pressure at a definite time as a function of the colatitude θ and longitude λ. Quite generally this function may be written as the series

$$Z(\theta\,\lambda) = \sum_{m=0}^{\infty}\sum_{n=m}^{\infty}\left[A_n^m \cos m\lambda + B_n^m \sin m\lambda\right] P_n^m(\theta)$$

$$= \sum_{m=0}^{\infty}\sum_{n=m}^{\infty} C_n^m\; P_n^m(\theta)\cos\left[m\lambda - \phi_n^m\right]$$

These series express an expansion of Z in terms of the spherical harmonics, where the functions P_n^m denote the Associated Legendre functions of the first kind, m means the number of waves round the earth, and (n-m) indicates the number of zero points between the north pole and the south pole. In the first form, A_n^m and B_n^m represent the spherical harmonic coefficients, while in the second form C_n^m is the amplitude and ϕ_n^m is the phase angle of the particular component, given by

$$C_n^m = \sqrt{A_n^{m^2} + B_n^{m^2}} \qquad\qquad \phi_n^m = \tan^{-1}\frac{B_n^m}{A_n^m}$$

The expansion is based upon the following condition of orthogonality

$$\int_{-1}^{+1} P_n^m(\mu)\,P_{n'}^m(\mu)\;d\mu = 0 \quad \text{if } n \neq n'$$
$$= 1 \quad \text{if } n = n'$$

and $\mu = \cos\theta$

When we use the Legendre functions normalized in this fashion, the normality factor becomes

$$\sqrt{\frac{2n+1}{2}\,\frac{(n-m)!}{(n+m)!}}$$

In terms of θ, the coefficients A_n^m and B_n^m are determined by the following integrals

$$A_n^m = \frac{1}{\delta_{ij}\pi}\int_0^{\pi}\int_0^{2\pi} Z(\theta,\lambda)\cos m\lambda \; P_n^m(\theta)\sin\theta \, d\theta \, d\lambda = \int_0^{\pi} A^m(\theta) \; P_n^m(\theta)\sin\theta \, d\theta$$
$$B_n^m = \frac{1}{\delta_{ij}\pi}\int_0^{\pi}\int_0^{2\pi} Z(\theta\,\lambda)\sin m\lambda \; P_n^m(\theta)\sin\theta \, d\theta \, d\lambda = \int_0^{\pi} B^m(\theta) \; P_n^m(\theta)\sin\theta \, d\theta \qquad (1)$$

where $A^m(\theta)$ and $B^m(\theta)$ are the usual Fourier coefficients and $\delta_{ij} = 1$ for $m > 0$ and $\delta_{ij} = 2$ for $m = 0$

Numerical Integration Methods

As we have the values Z only at a network of points over the sphere, the coefficients $A^m(\theta)$, $B^m(\theta)$ and A_n^m, B_n^m can be evaluated from their integral formulae only by means of quadrature sums. $A^m(\theta)$ and $B^m(\theta)$ are evaluated simply by the Trapezoidal rule, using 36 equally spaced values around each latitude circle chosen, in which way the coefficients for $m \angle 36$ will be the same as the coefficients determined by the method of least squares, regardless of the number of harmonics used to fit the function. In order to evaluate the integrals in (1), the following three methods have been tested,

(i) Gaussian quadrature formula

(ii) Simpson and Trapezoidal rules

The general numerical form of (1) for colatitude values of $\theta_i = 1$ to $\theta_i = 37$ is as follows,

$$A_n^m = \frac{\pi}{36}\sum_{i=1}^{37} A^m(\theta_i) \; P_n^m(\theta_i)\sin\theta_i \, w_i$$
$$B_n^m = \frac{\pi}{36}\sum_{i=1}^{37} B^m(\theta_i) \; P_n^m(\theta_i)\sin\theta_i \, w_i \qquad (2)$$

where w_i is the weighting function which varies for different methods of quadrature.

(i) Gaussian Formula

For the integration of the function $f(\mu)=A^m(\mu)P_n^m(\mu)$ we have

$$\int_{-1}^{+1} f(\mu)\,d\mu=\sum_{k=1}^{k=K} A^m(\mu_k)\,P_n^m(\mu_k)\,G_k \tag{3}$$

where μ_k are the roots of the Legendre polynomial (P_K^o) and G_k the corresponding Gaussian weights. This quadrature formula is of the highest algebraic degree of precision, i.e., it is exact for $f(\mu)$ being any polynomial of degree smaller or equal to 2K-1.

Using the Gauss formula with K=20, we then obtain

$$\begin{aligned} A_n^m &= \sum_{k=1}^{20} A^m(\mu_k)\,P_n^m(\mu_k)\,G_k \\ B_n^m &= \sum_{k=1}^{20} B^m(\mu_k)\,P_n^m(\mu_k)\,G_k \end{aligned} \tag{4}$$

In order to compute A_n^m and B_n^m from the expressions (4), $A^m(\mu)$ and $B^m(\mu)$ as well as $P_n^m(\mu)$ must be determined at the latitudes corresponding to μ_k. Since the heights were not extracted at these latitudes, values for $A^m(\mu)$ and $B^m(\mu)$ were obtained by a four point Lagrangian interpolation. In each interpolation, the 4 nearest points were chosen as follows,

$$\begin{aligned} f(\mu_k) = {} & \frac{(\mu_k-\eta_2)(\mu_k-\eta_3)(\mu_k-\eta_4)}{(\eta_1-\eta_2)(\eta_1-\eta_3)(\eta_1-\eta_4)} f(\eta_1) + \frac{(\mu_k-\eta_3)(\mu_k-\eta_4)(\mu_k-\eta_1)}{(\eta_2-\eta_3)(\eta_2-\eta_4)(\eta_2-\eta_1)} f(\eta_2) \\ & + \frac{(\mu_k-\eta_4)(\mu_k-\eta_1)(\mu_k-\eta_2)}{(\eta_3-\eta_4)(\eta_3-\eta_2)(\eta_3-\eta_1)} f(\eta_3) + \frac{(\mu_k-\eta_1)(\mu_k-\eta_2)(\mu_k-\eta_3)}{(\eta_4-\eta_1)(\eta_4-\eta_2)(\eta_4-\eta_3)} f(\eta_4) \end{aligned}$$

where $f(\mu_k)$ is the interpolated value of the polynomial at μ_k and $f(\eta_1)$, $f(\eta_2)$, $f(\eta_3)$, $f(\eta_4)$ are the known values of the polynomial at the four nearest points $\eta_1, \eta_2, \eta_3, \eta_4$.

(ii) Simpson's and Trapezoidal Rules

The Trapezoidal rule requires ω_i to have the following 37 values $\omega_1 = \omega_2 = \omega_3 = \omega_4 = \cdots\cdots = \omega_{37} = 1$

Simpson's rule uses the weights,

$$\omega_1 = \omega_{37} = \frac{1}{3}; \quad \omega_2 = \omega_4 = \omega_6 = \cdots\cdots = \omega_{36} = \frac{4}{3}$$
$$\omega_3 = \omega_5 = \omega_7 = \cdots\cdots = \omega_{35} = \frac{2}{3}$$

Interpreted geometrically, Simpson's rule gives the value of the sum of the areas under second degree parabolas, while the Trapezoidal rule gives the sum of the areas of the trapezoids; it would then apply best to a first degree polynomial.

Computation of Variance

In the following, expressions are derived for the variance of the height field, the mean variance of the flow and the variance of the mean flow. These are used to compute the fluctuating variance of the flow.

If we let $Z(\theta,\lambda)$ represent the height at (θ,λ) and $\bar{Z}$ be the mean height over the globe, then the deviation from the mean is given by

$$Z'(\theta,\lambda) = Z(\theta,\lambda) - \bar{Z}$$

and the variance would be

$$\sigma^2 = \frac{1}{4\pi} \int_0^{2\pi}\int_0^{\pi} Z'^2 \sin\theta \, d\theta \, d\lambda$$

but we have

$$Z(\theta,\lambda) = \sum_{n=0}^{15} A_n^0 P_n^0 + \sum_{n=1}^{15}\sum_{m=1}^{n} \left[A_n^m \cos m\lambda + B_n^m \sin m\lambda\right] P_n^m(\theta)$$

and $\bar{Z} = A_0^0 P_0^0$ so that

$$Z'(\theta,\lambda) = \sum_{n=1}^{15} A_n^0 P_n^0 + \sum_{n=1}^{15}\sum_{m=1}^{n}\left[A_n^m \cos m\lambda + B_n^m \sin m\lambda\right] P_n^m(\theta)$$

Hence

$$\sigma^2 = \frac{1}{4\pi}\int_0^{\pi}\int_0^{2\pi}\left[\sum_{n=1}^{15} A_n^0 P_n^0\right]^2 \sin\theta\, d\theta\, d\lambda$$

$$+2\int_0^{\pi}\int_0^{2\pi}\sum_{n=0}^{15} A_n^0 P_n^0 \sum_{n=1}^{15}\sum_{m=1}^{n}\left[A_n^m \cos m\lambda + B_n^m \sin m\lambda\right]\sin\theta\, d\theta\, d\lambda$$

$$+\int_0^{\pi}\int_0^{2\pi}\left[\sum_{n=1}^{15}\sum_{m=1}^{15}\left[A_n^m \cos m\lambda + B_n^m \sin m\lambda\right] P_n^m\right]^2 \sin\theta\, d\theta\, d\lambda$$

By the use of the orthogonality property, we obtain

$$\sigma^2 = \frac{1}{2}\sum_{n=1}^{15}\left[A_n^0\right]^2 + \frac{1}{4}\sum_{n=1}^{15}\sum_{m=1}^{n}\left[A_n^{m^2} + B_n^{m^2}\right]$$

The variance of a single component is

$$\sigma_n^{0^2} = \frac{1}{2} A_n^{0^2} \qquad 0 \leq n \leq 15$$

and

$$\sigma_n^{m^2} = \frac{1}{4}\left[A_n^{m^2} + B_n^{m^2}\right] \qquad 1 \leq m \leq n \leq 15$$

To obtain the fluctuating variance $\sigma_{Fn}^{m^2}$ we denote the mean over the month of A_n^m and B_n^m by $\overline{A_n^m}^t$ and $\overline{B_n^m}^t$ respectively, then

$$\sigma_{Fn}^{m^2} = \frac{1}{4}\left[\frac{1}{30}\sum_{i=1}^{30}\left[A_{in}^m - \overline{A_n^m}^t\right]^2 + \frac{1}{30}\sum_{i=1}^{30}\left[B_{in}^m - \overline{B_n^m}^t\right]^2\right]$$

$$= \frac{1}{4}\left[\frac{1}{30}\sum_{i=1}^{30}\left[A_{in}^{m\,2} - \overline{A}_{n}^{m\,t\,2}\right] + \left[B_{in}^{m\,2} - \overline{B}_{n}^{m\,t\,2}\right]\right]$$

$$= \frac{1}{4}\left[\frac{1}{30}\sum_{i=1}^{30}\left[A_{in}^{m\,2} + B_{in}^{m\,2}\right] - \left[\overline{A}_{n}^{m\,t\,2} + \overline{B}_{n}^{m\,t\,2}\right]\right]$$

where i is a time index, the first bracketed term on the right hand side is the mean monthly variance (mean variance of the flow) and the second bracketed term is the variance of the mean flow. Thus a small value of $\sigma_{Fn}^{m\,2}$ indicates a strong stationary component.

In the case of the zonal components, the mean monthly variance is given by

$$\frac{1}{2}\left[\frac{1}{30}\sum_{i=1}^{30} A_{in}^{o\,2}\right]$$

ANALYSIS OF ERRORS

The errors involved in the calculation of the variance and phase angle are due to the following sources,

(1) Measurement of the parameters.

(2) Chart Analysis.

(3) Gross errors of data extraction and card punching.

(4) Interpolation of the pressure values to grid points.

(5) Numerical integration method.

(1) Measurement errors in surface pressure and temperature are very small. Pressure is reported to 1/10 of a mb and temperature is reported to a whole degree.

(2) Chart analysis errors generally tend to decrease the variance of the field and in particular that contained in the shorter waves. This type of error is most serious in areas with sparse data.

(3) Errors in data extractions and card punching were readily recognized by spurious amplitude variations in the high Fourier wave numbers. It is considered that all significant errors of this type have been eliminated.

(4) The error caused by interpolating the pressure values to grid-points is estimated to be $\pm$ 0.5 mb and for temperature $\pm$ 5.0°C. These introduce the following error in the height calculation, at a grid point, of the 1000 mb level.

We have, from theory,

$$Z(\theta,\lambda) = \frac{R_d}{g} T \ln \frac{P(\theta,\lambda)}{P_c}$$

$$dZ = \frac{R_d}{g}\left[T d\ln \frac{P}{P_c} + \ln \frac{P}{P_c} dT\right]$$

i.e.

$$\Delta Z = \frac{287}{9.8}\left[T \frac{\Delta P}{P} + \ln \frac{P}{P_c} \Delta T\right]$$

If we choose the following reasonable values,

$P=1025$ mb	$\Delta P=\pm\ 0.5$ mb
$T=300^{\circ}K$	$\Delta T=\pm\ 5^{\circ}C$

we obtain $\Delta Z=\pm\ 0.75$ dm

The error in Z is mainly pressure dependent.

(5) Accuracy of the Numerical Integration Techniques

The accuracy of the Trapezoidal, Simpson and in part the Gaussian methods of quadrature have been investigated in the present study. Physically real input values of spherical harmonic coefficients A_n^m were chosen to generate a global height field of the 1000 mb level. This field was in turn used to recalculate the harmonic coefficients. The percent deviation between the input and output field should give a measure of the accuracy of the integration method. Table 1 presents the input coefficients, while Tables 2, 3 and 4 show the percent deviation of the output from the input coefficients as obtained by the Trapezoidal, Simpson and Gaussian methods, respectively. The results are tabulated only to two decimal places.

Simpson's rule appears to be more accurate for the zonal components and the Trapezoidal method is slightly better for the wave components. The difference which occurs mainly in the third decimal digit of the wave components is not shown in the tables.

Table I

Input of the spherical harmonic coefficients A_n^m

n / m	0	1	2	3	4	5	6	7	8	9	10	11	12	13	14	15
0	14.26	1.97	-4.00	3.98	-3.82	-0.85	1.06	-0.73	0.68	-0.90	0.48	-1.19	0.52	-0.33	-0.20	-0.29
1		1.62	1.02	1.29	1.77	0.99	-0.73	-0.55	-0.95	0.47	0.75	0.34	0.42	0.10	-0.08	0.02
2			0.57	0.13	-0.59	-2.22	-0.91	-0.96	-0.30	0.82	-0.43	0.73	-0.65	0.25	-0.08	-0.19
3				-0.65	1.05	-1.34	2.02	-0.71	0.36	-0.81	-0.33	-0.44	0.34	-0.09	0.48	0.14
4					0.43	0.30	0.00	1.22	-0.42	0.52	0.24	-0.18	0.63	0.02	-0.00	0.13
5						0.23	-1.44	0.30	-1.19	0.53	0.20	0.02	-0.02	0.04	-0.18	0.20
6							0.18	0.27	-0.07	0.69	0.29	0.96	0.30	0.03	0.10	-0.39
7								0.73	-1.64	0.90	-1.67	0.12	-0.76	-0.60	-0.03	-0.57
8									0.07	-0.79	-0.23	-0.14	0.18	0.33	0.07	0.31
9										-0.13	0.11	-0.45	0.39	-0.51	0.00	-0.38
10											-0.07	-0.23	-0.11	-0.08	-0.06	0.26
11												0.01	0.04	-0.22	0.06	-0.39
12													0.00	0.26	0.02	0.30
13														-0.07	0.05	-0.04
14															-0.08	0.19
15																-0.03

Table 2

Percent deviation of the spherical harmonic coefficient A_n^m

from the input A_n^m by the Trapezoidal Rule

m \ n	0	1	2	3	4	5	6	7	8	9	10	11	12	13	14	15
0	0.02	-0.32	-0.16	-0.23	-0.22	1.30	0.95	1.73	1.70	1.57	2.70	1.32	2.75	5.13	-7.38	1.61
1		-0.00	-0.00	-0.01	-0.00	-0.02	0.01	0.04	0.02	-0.08	-0.03	-0.14	-0.07	-0.58	0.92	-3.14
2			0.00	0.00	0.00	-0.00	0.00	-0.00	0.00	0.00	0.00	0.00	0.00	-0.01	0.05	-0.00
3				0.00	0.00	0.00	0.00	0.00	0.00	0.00	0.00	0.00	-0.00	-0.00	0.00	-0.00
4					0.00	0.00	0.01	0.00	0.00	0.00	0.00	-0.00	0.00	0.00	0.02	-0.00
5						0.00	0.00	0.00	0.00	0.00	0.00	0.00	0.00	0.00	0.00	-0.00
6							0.00	0.00	-0.00	0.00	0.00	0.00	0.00	0.00	0.00	0.00
7								0.00	0.00	0.00	0.00	0.00	0.00	0.00	0.00	0.00
8									0.00	0.00	-0.00	0.00	0.00	0.00	-0.00	0.00
9										-0.00	0.00	0.00	0.00	0.00	0.00	0.00
10											-0.00	0.00	-0.00	0.00	-0.00	0.00
11												-0.01	-0.00	-0.00	0.00	0.00
12													-0.00	0.00	0.00	0.00
13														-0.00	-0.00	-0.00
14															-0.00	-0.00
15																-0.00

Table 3

Percent deviation of the spherical harmonic coefficient A_n^m

from the input A_n^m by Simpson's Rule

m \ n	0	1	2	3	4	5	6	7	8	9	10	11	12	13	14	15
0	-0.00	0.06	0.01	0.06	0.03	-0.49	-0.14	-0.86	-0.34	-0.99	-0.71	-1.07	-0.96	-5.80	4.25	-14.87
1		0.01	0.01	0.03	0.02	0.08	-0.08	-0.24	-0.10	0.45	0.20	0.93	0.56	5.02	-4.09	35.39
2			0.00	-0.01	-0.01	0.00	-0.02	0.01	-0.11	-0.02	-0.15	-0.04	-0.19	-0.20	-2.96	0.39
3				0.00	0.00	0.00	0.00	0.00	0.01	0.00	-0.03	0.01	0.08	0.06	0.15	-0.02
4					0.00	-0.00	0.00	0.00	0.00	-0.00	-0.00	0.01	-0.00	-0.17	1.90	-0.11
5						0.00	0.00	0.00	0.00	0.00	-0.00	0.02	0.02	0.04	0.01	0.03
6							0.00	0.00	-0.00	0.00	0.00	0.00	-0.00	0.02	-0.00	-0.01
7								0.00	0.00	0.00	0.00	0.00	0.00	0.00	0.00	0.00
8									0.00	0.00	-0.00	0.00	0.00	-0.00	-0.00	-0.00
9										-0.00	0.00	0.00	0.00	0.00	0.00	0.00
10											-0.00	0.00	-0.00	0.00	-0.00	0.00
11												-0.01	-0.00	-0.00	0.00	0.00
12													-0.00	0.00	0.00	0.00
13														-0.00	-0.00	-0.00
14															-0.00	-0.00
15																-0.00

Table 4

Percent deviation of the spherical harmonic coefficients A_n^m from the input A_n^m by the Gaussian method

m \ n	0	1	2	3	4	5	6	7	8	9	10	11	12	13	14	15
0		0.54	0.15	0.23	-0.02	-0.42	0.35	1.02	0.62	1.31	0.48	-0.10	-2.12	-0.16	0.27	2.22

The table also shows that the Trapezoidal method gives an over-estimate of the values of the coefficients exactly where Simpson's rule gives an underestimate and vice-versa. For practical applications, the two methods can be considered equivalent since the actual error involved does not add much to the noise-level, which is mainly created by error 2) discussed above.

The percent deviation by the Gaussian formula (with a four point Lagrangian interpolation) was computed only for the zonal components. It seems to be superior to Simpson's rule for $n \gtrsim 10$ but inferior for $n \lesssim 10$. Since components with smaller n are more important, Simpson's rule was used to obtain the zonal harmonic coefficients.

Noise Level.

The random error of $\pm$ 0.75 dm in the height computation at a grid point introduces a very small error (about 10^{-4} dm^2) in the variance of an individual component and is thus considered insignificant. Also errors 1) and 5) are considered insignificant. The errors of chart analysis are the most serious and the main contributors to the noise-level. Since they are random in nature, it becomes very difficult to include them in the computations of the variance and phase angle. By considering the output results, one can make a reasonably satisfactory estimate of the noise level. The underlying assumption is that no large jumps in the phase angle of a low order component exist in the real atmosphere at the 1000 mb level. Hence a sequence of erratic and large phase changes can only occur if the variance is in the noise level. This in fact seems to occur in all the components.

The deciding factor in choosing a lower limit for the value of the variance below which the wave would not be considered significant was selected from the behaviour of the component (1, 4) which is seen to have very high variance values during the month.

The variance of $(m, n) = (1, 4)$ was relatively large for the first 25 days of the month and the wave exhibited mainly small fluctuations about a mean position. However, on September 27, the variance dropped to 0.27 dm^2 and the phase change in the period from September 26 to 28 was large. Thus a choice of 0.27 dm^2 as the lowest limit of significant values of the variance is quite a high value which eliminates the physically unreal variances, but may at times eliminate some small but physically real values of the variance.

ANALYSIS OF VARIANCE

Spectral Distribution of the Variance

On the basis of the spherical-harmonic analysis of the height field we may now, as a fundamental characteristic, consider the spectral distribution of the variance which is a measure of the importance of the different components in the spherical harmonic representation.

The mean values of $\sigma_n^{m\,2}$ at the 1000 mb level for September 1957 are shown in Table 5 for $m \leq 15$ and $n-m \leq 15$. Expressed in percent, table 6 shows that the largest individual contributions are found for the components with the smaller m and n, i.e. for the harmonics of the largest scales. Thus, the contributions from the zonal flow, $m = 0$ are together about 60 per cent and the contributions from wave numbers, 1, 2, 3 and 4 are together about 31 per cent of the total contribution from all the components in the table. It is seen that the most dominant components in table 5 are the odd tesseral harmonics (1, 4) and (2, 5).

Summations of the mean monthly variance over n for every m and over m for every n for the wave components have been included in table 5. When plotted in the form of histograms in Figures 2a), b) and c), they illustrate the spectral distribution of the variance. In Figure 2a), $m = 1$ has the largest amount of

Table 5

Mean monthly variance of the spherical harmonic components

for September 1957 (Dm^2)

m \ n	1	2	3	4	5	6	7	8	9	10	11	12	13	14	15	Sum
0	4.84	9.34	11.86	6.68	0.34	2.40	0.74	1.34	0.17	0.08	0.13	0.13	0.03	0.06	0.04	
1	1.36	0.44	0.62	1.76	0.41	0.44	0.23	0.82	0.32	0.12	0.12	0.09	0.04	0.05	0.03	6.84
2		0.51	0.40	0.52	1.78	0.48	0.52	0.26	0.52	0.18	0.21	0.15	0.11	0.06	0.05	5.75
3			0.18	0.19	0.45	0.61	0.50	0.35	0.25	0.20	0.16	0.11	0.06	0.06	0.04	3.17
4				0.30	0.73	0.52	0.92	0.38	0.43	0.39	0.16	0.10	0.08	0.05	0.05	4.11
5					0.15	0.23	0.30	0.28	0.31	0.26	0.12	0.10	0.08	0.07	0.07	1.98
6						0.07	0.10	0.18	0.30	0.13	0.15	0.12	0.07	0.06	0.04	1.22
7							0.08	0.16	0.15	0.19	0.12	0.10	0.07	0.05	0.04	0.96
8								0.04	0.21	0.05	0.08	0.09	0.06	0.05	0.04	0.52
9									0.01	0.06	0.05	0.08	0.06	0.04	0.05	0.35
10										0.01	0.03	0.03	0.04	0.05	0.04	0.19
11											0.01	0.02	0.02	0.02	0.02	0.09
12												0.00	0.01	0.02	0.01	0.05
13													0.01	0.01	0.01	0.02
14														0.00	0.01	0.01
15															0.00	0.00
Sum	1.36	0.95	1.20	2.77	3.52	2.36	2.64	2.47	2.40	1.58	1.21	0.99	0.71	0.59	0.50	

Note: Summation of the mean monthly variance over m and n respectively does not include the zonal components.

Table 6

Mean monthly variance of the spherical harmonic components

expressed in percent of the total mean monthly variance

m \ n	1	2	3	4	5	6	7	8	9	10	11	12	13	14	15	Total
0	7.62	14.72	18.70	10.53	0.53	3.78	1.16	2.11	0.26	0.13	0.21	0.21	0.04	0.10	0.07	60.17
1	2.14	0.69	0.98	2.78	0.65	0.69	0.36	1.30	0.50	0.18	0.19	0.14	0.06	0.08	0.04	10.78
2		0.81	0.63	0.81	2.80	0.76	0.82	0.41	0.83	0.29	0.33	0.24	0.17	0.09	0.08	9.07
3			0.29	0.30	0.71	0.97	0.79	0.54	0.39	0.32	0.26	0.17	0.10	0.09	0.07	5.00
4				0.47	1.16	0.82	1.45	0.61	0.68	0.61	0.25	0.16	0.13	0.07	0.08	6.49
5					0.24	0.36	0.47	0.44	0.49	0.41	0.19	0.16	0.13	0.11	0.11	3.11
6						0.11	0.16	0.28	0.47	0.21	0.23	0.18	0.11	0.10	0.06	1.91
7							0.12	0.26	0.24	0.31	0.19	0.16	0.10	0.08	0.06	1.52
8								0.06	0.17	0.08	0.13	0.14	0.10	0.08	0.06	0.84
9									0.02	0.09	0.08	0.12	0.10	0.07	0.08	0.56
10										0.01	0.04	0.05	0.06	0.07	0.06	0.29
11											0.01	0.03	0.03	0.03	0.04	0.14
12												0.01	0.02	0.03	0.02	0.08
13													0.01	0.01	0.02	0.04
14														0.00	0.01	0.01
15															0.00	0.00

Note: The total zonal mean field and the waves with longitudinal wavenumber 0 to 4 represent 91.5 per cent of the total variance.

variance and $m = 2$ is the next in magnitude, partly because the lower m indices contain more n indices and the number of (m, n) components decreases as m increases. Figure 2c) has been added to illustrate the variance as a function of the meridional dimensions of the waves. Predominant in this distribution are the components with $n-m=3$. This has a remarkable resemblance to the same type of distribution presented by Steinberg for the 500 mb level (see Figure 2d). It thus appears that components $n-m=3$ contain the largest amount of variance at the two levels, the magnitude being greater at 500 mb surface.

Stationary and Travelling Long Waves

To study quantitatively the standing waves in the atmosphere, we may consider the spectral distribution of the fluctuating variance as given in Table 7. Since these values are positive, it is understood that the contributions of the variances of the mean flow are smaller than the mean values presented in table 5, particularly so for components with larger m and n, i.e. for components with smaller scales. The fluctuating variance is most physically meaningful for components which have a large mean monthly variance. In this category, we find the components with (m, n) = (1, 1), (1, 4), (1, 6), (1, 8) and (2, 5). In table 7, these components are found to have small values of fluctuating variance, illustrating their semi-permanent character. The most stationary of all the harmonics are (1, 1), (1, 4) and (2, 5); their fluctuating variances are 23.5, 31.3 and 34.0 percent of the mean variance, respectively.

Graphically one can separate the stationary and travelling modes of a planetary wave by Deland's two component model. The amplitude and phase angle of the harmonics (1, 1), (1, 4), (1, 8) and (2, 2), (2, 5), (2, 7) are plotted for every day of the month on polar diagrams in Figures 3a), b), c) and 4a), b), c) respec-

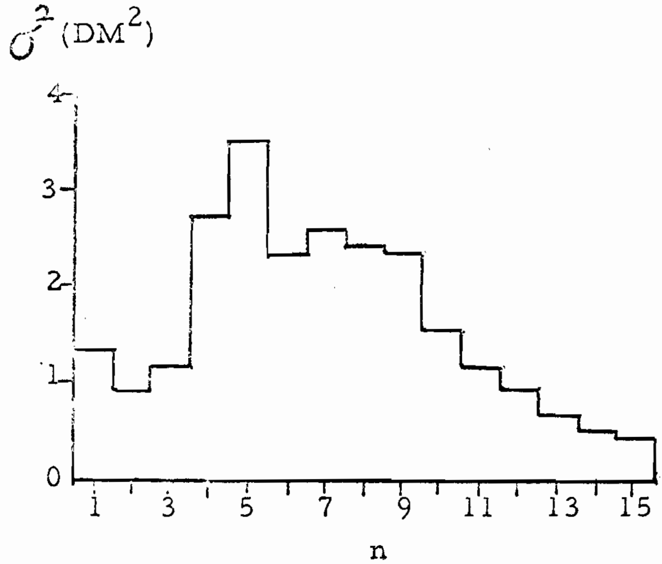

(b) The mean monthly variance shown as a function of n(the two dimensional wave number).

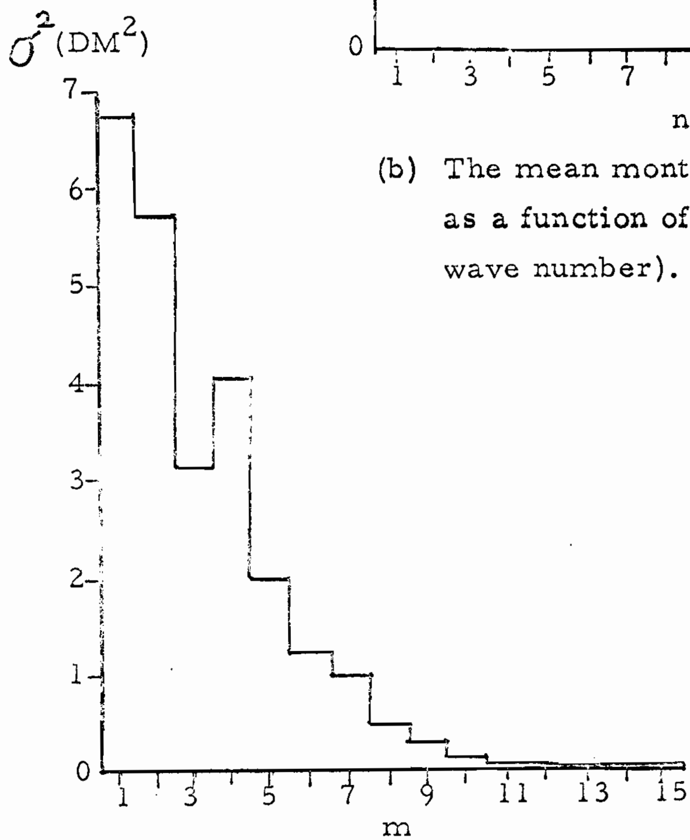

(a) The mean monthly variance shown as a function of m (the longitudinal wave number).

Figure 2. Spectral distribution of the mean monthly variance.

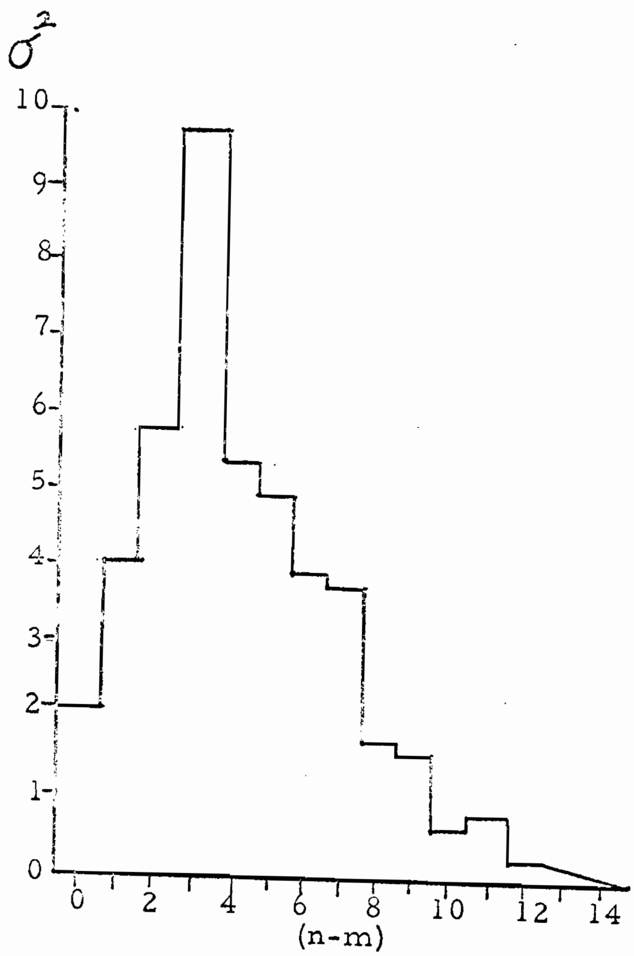

(d) The mean monthly variance shown as a function of (n-m) (latitudinal wave number).

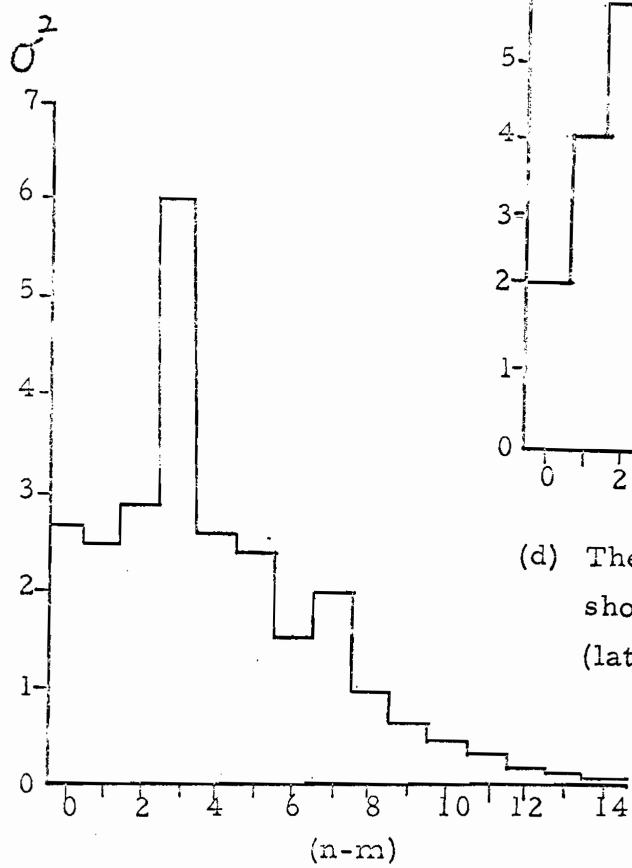

(c) The mean monthly variance shown as a function of (n-m) (the latitudinal wave number) at the 1000 mb level.

Figure 2. Spectral distribution of the mean monthly variance in the meridional direction.

Table 7

Percent of the fluctuating variance of the spherical harmonic components for September 1957 (Dm^2)

m \ n	1	2	3	4	5	6	7	8	9	10	11	12	13	14	15
1	23.51	82.98	86.72	31.33	91.09	61.48	90.96	26.15	25.64	81.37	85.62	95.87	99.13	75.94	97.97
2		38.84	64.82	91.00	34.01	77.35	85.66	89.77	32.75	65.12	62.52	74.54	41.76	96.15	78.25
3			51.41	96.93	95.36	92.53	98.51	92.03	87.83	76.93	99.60	73.24	98.34	99.83	77.54
4				31.11	57.36	94.02	90.52	81.31	83.97	40.72	74.14	90.00	83.58	97.47	93.07
5					36.95	63.22	99.68	97.77	96.39	81.60	91.43	87.28	80.84	86.48	67.90
6						41.97	98.17	71.04	69.66	87.45	90.19	85.07	92.81	99.35	83.09
7							27.25	63.68	83.75	98.85	91.67	88.39	98.58	89.67	86.31
8								41.49	43.22	96.06	95.98	96.08	99.43	94.85	99.60
9									66.85	48.52	85.30	99.40	97.89	97.83	97.33
10										73.10	57.98	95.81	83.03	88.78	93.88
11											56.02	57.66	94.42	90.89	62.70
12												91.43	63.33	96.79	91.62
13													53.32	98.03	99.51
14														71.25	97.05
15															96.12

Note: Among the long waves, those for which table 5 indicates a large mean monthly variance, the present table indicates a small fluctuating variance.

tively. In the case of the lower harmonics, it is apparent that the wave vector does not describe a circle around the pole as it should in the case of a single wave, but instead it follows a roughly circular path as if it represented a travelling planetary wave superimposed on a quasi stationary wave. In figure 3a) for (m, n) = (1, 1), the travelling wave retrogresses (clockwise motion) in a disorganized manner due to the large changes of its amplitude. Thus, it seems more convenient to break this eccentric circular path of 30 days into a number of almost complete circular motions. This travelling planetary wave seems to retrogress around a mean position for the first 6 days, then decreases greatly in amplitude and again retrogresses around another centre for about 5 days, then increases in amplitude greatly and again retrogresses around a different centre for another 5 days (until the 18th day); the monthly motion is completed by another retrogressive cycle. This graph illustrates 4 main cycles of westward motion; the centre of each cycle may be considered to be the position vector of the quasi-stationary component and this shows a slow retrogressive motion over the month. For (m, n) = (1, 4) in figure 3b), we see a major cycle of retrogressive motion (clockwise) about a mean position for the first 10 days, then a large drop in amplitude, followed by a progressive cycle (anti clockwise) between the 13th and the 18th days; the motion seems to end with another progressive cycle. In the case of component (1, 8) which is a small scale wave in the north-south direction, the major cycles exhibit progressive motion.

The above description seems to indicate that the largest scale planetary wave (1, 1) is completely described by a retrogressive travelling wave superimposed on a fixed wave, while for increasing n (decreasing north-south dimensions) the number of cycles of a progressive travelling wave increases. This picture seems to repeat itself in the analysis of a similar set of components in figures 4a), b) and c). Harmonic (2, 2) is described only by a retrogressive travelling wave, (2, 5) clearly shows a cycle of eastward motion for the first 11 days, a cycle of retrogression between the 12th and 19th days and a final progressive cycle between the 20th and the 30th days. Finally (2, 7) is totally described by 3 cycles of eastward motion. We also note that the stationary component of (2, 2) is as pronounced as that of (1, 1). It should be mentioned that when the amplitude is very small (in the noise level), the phase angle loses its physical meaning.

One implication of the above discussion is that the latitudinal (represented by n-m or n), as well as the longitudinal (represented by m) scale should be taken into account in a scale analysis of planetary waves.

As a final illustration of the quasi-stationary character of the large scale waves, figures 5a) and b) are presented. It is clearly seen that the large scale features on the mean map (figure 5a)) are very similar to the flow pattern described by the superposition of the components $0 \leq m \leq 4$ and $m \leq n \leq 10$. The main features on the mean map are a Low over Scandinavia (15° E) which extends west to Iceland (20° W), a High over Asia (centred at about 80° E), a Low over the Pacific (160° W) and a ridge over Western Canada (110° W). The same disturbances appear at almost the same geographical location in figure 5b) (which includes only the ultra-long longitudinal waves of September 1), except for the ridge over Western Canada which is not as pronounced as that of the mean map. Thus, the long waves which appeared on the map of September 1st show up clearly on the mean map.

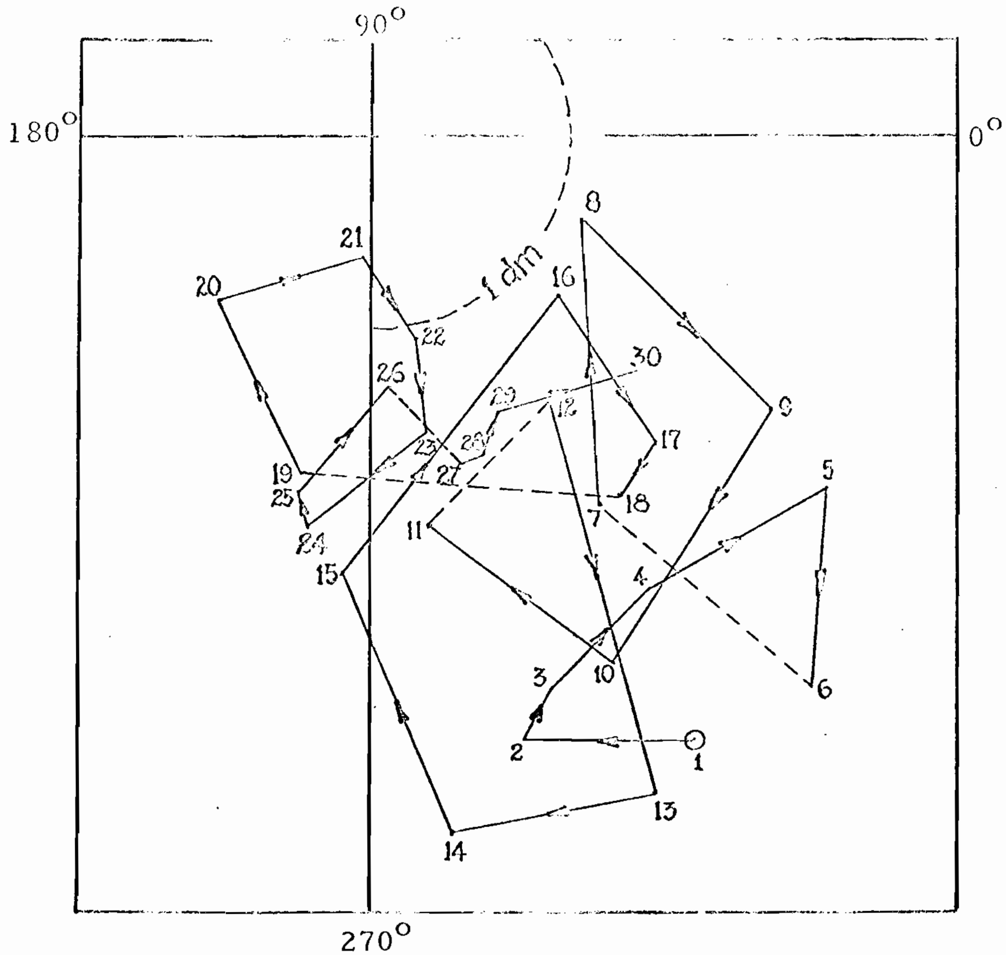

Figure 3a. Daily values of the harmonic (1, 1) plotted on a polar diagram; each point represents one day. The graph shows cycles of retrogressive (clockwise) motion only. The average rotation period is 5 days.

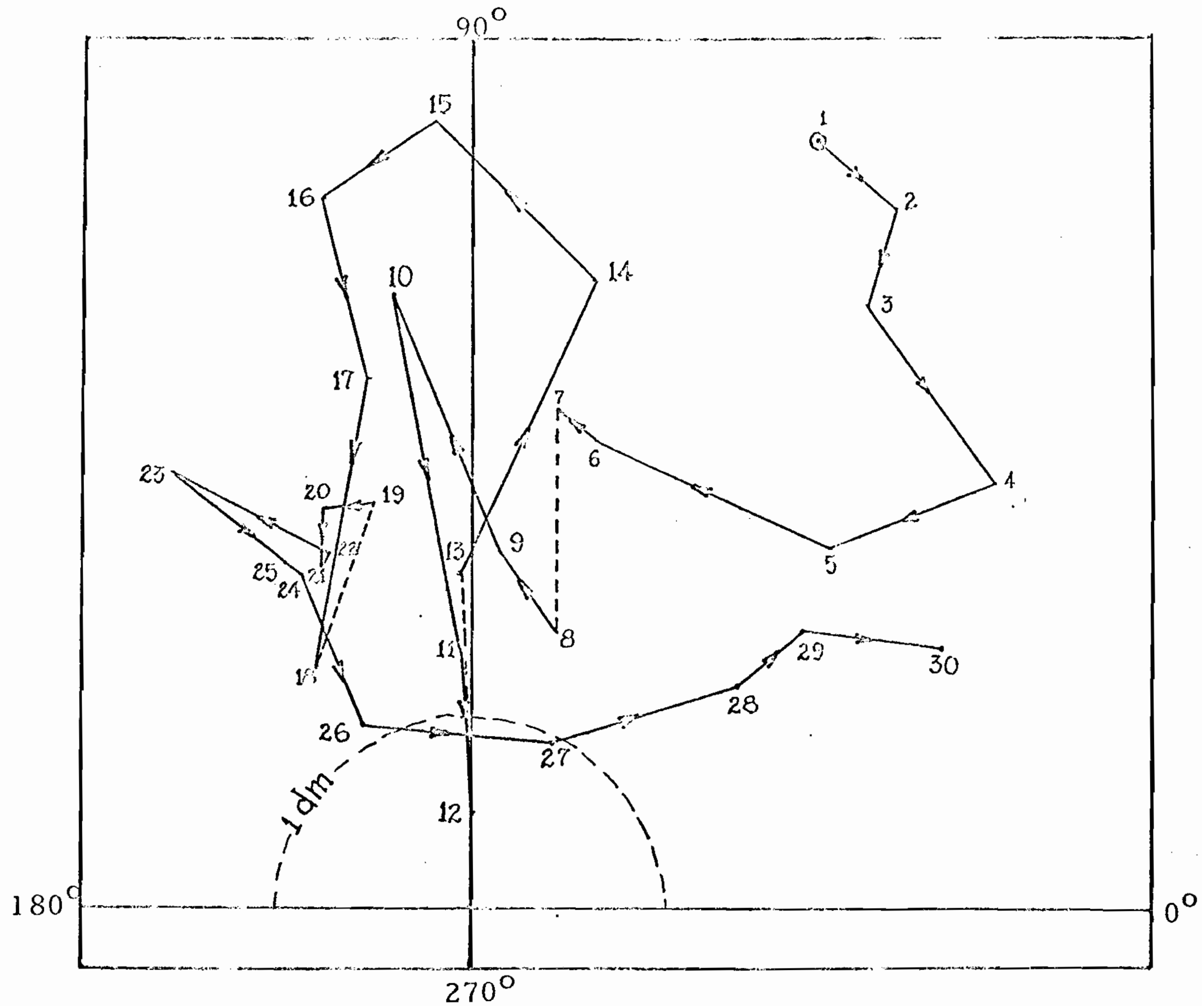

Figure 3b. Daily values of the harmonic (1,4) plotted on a polar diagram; each point represents one day. This component shows more progressive (anticlockwise) cycles than component (1, 1).

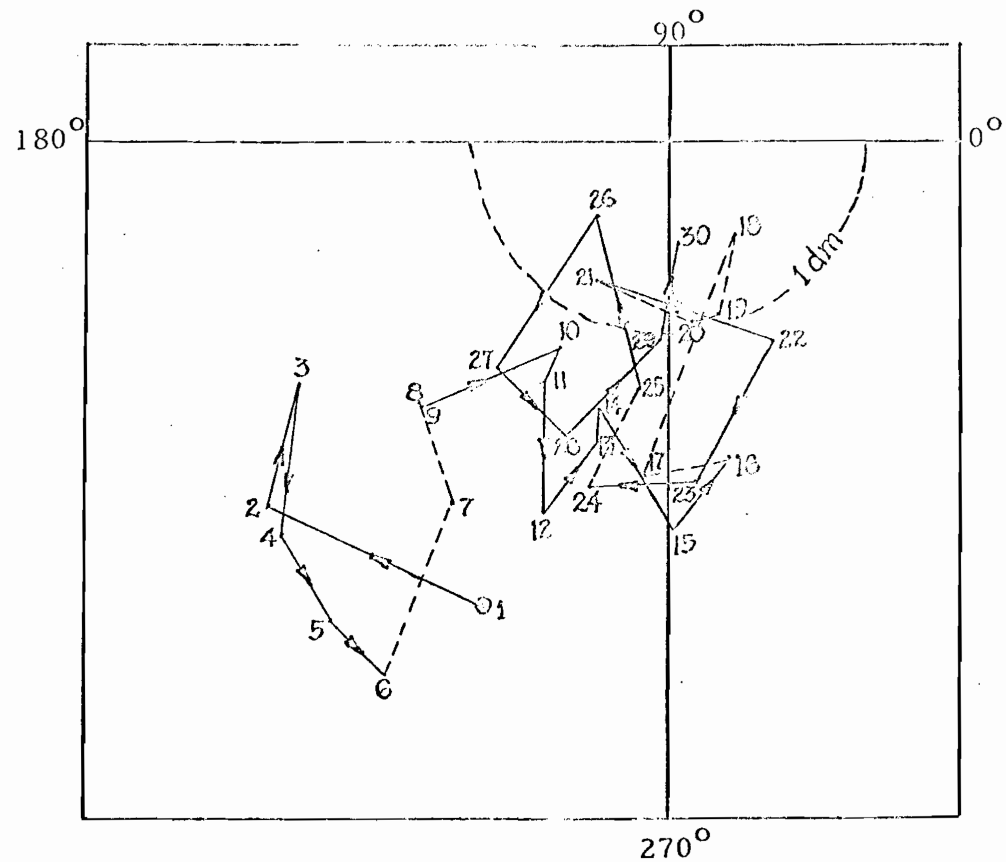

Figure 3c. Daily values of harmonic (1, 8) plotted on a polar diagram. The amplitudes for most of the days are small; however, the days for which the amplitude has physical significance, the motion is more progressive (anticlockwise) than was found for harmonic (1, 4).

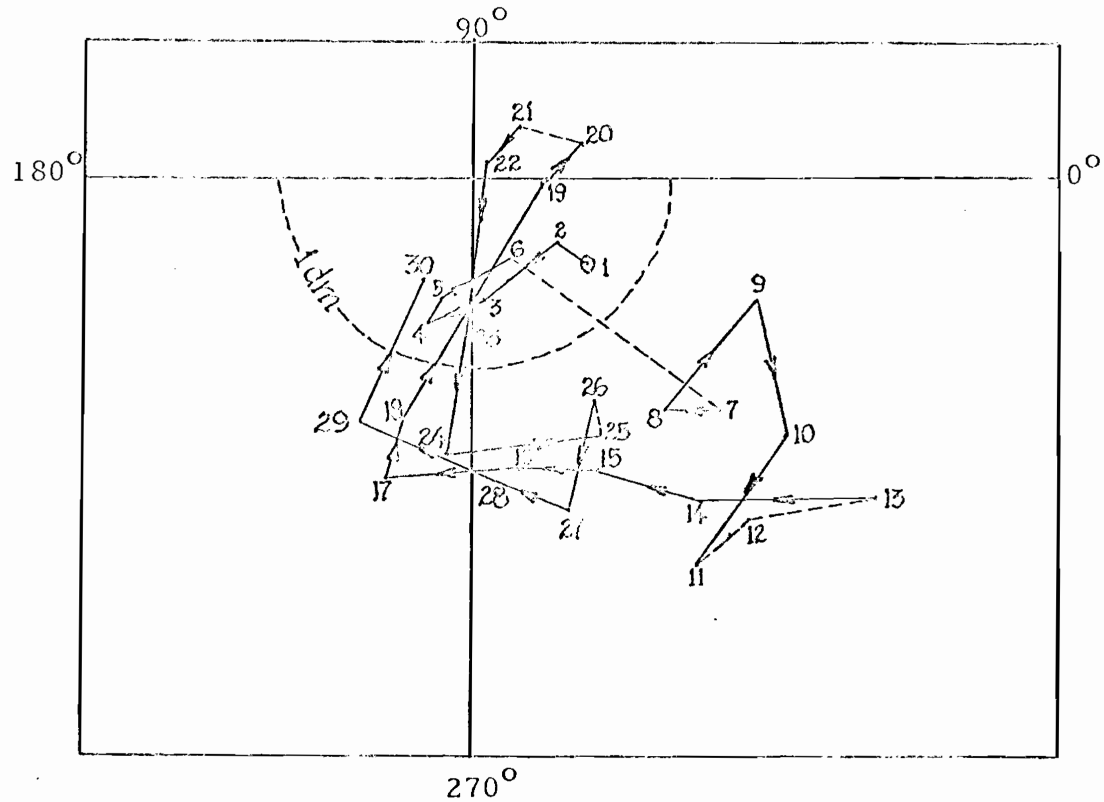

Figure 4a. A polar diagram for harmonic (2, 2); each point represents one day. The graph illustrates cycles of retrogressive (clockwise) motion, as is the case with the long wave (1, 1).

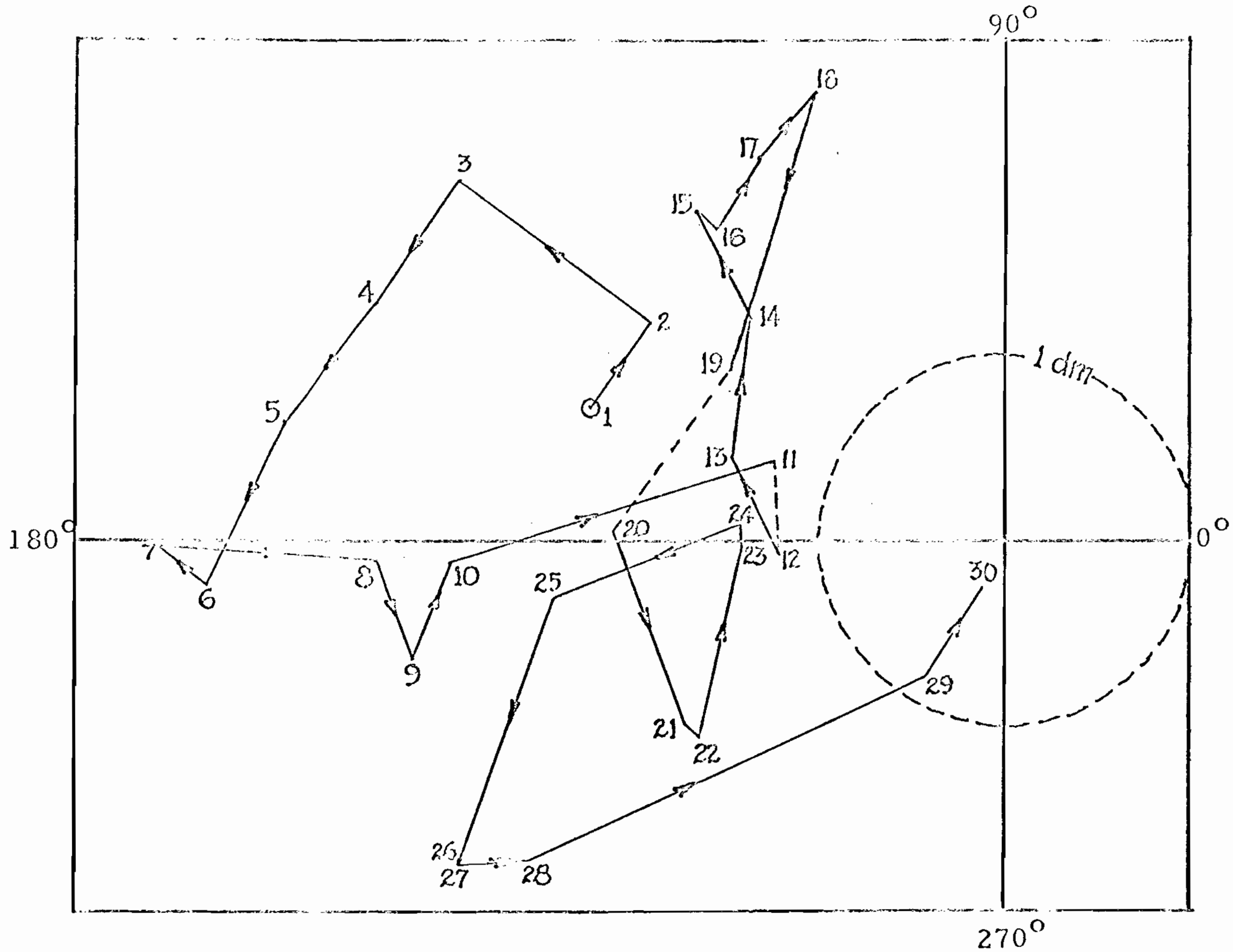

Figure 4b. A polar diagram for harmonic (2, 5). It illustrates two major cycles of progressive (anticlockwise) motion, similar to component (1, 4).

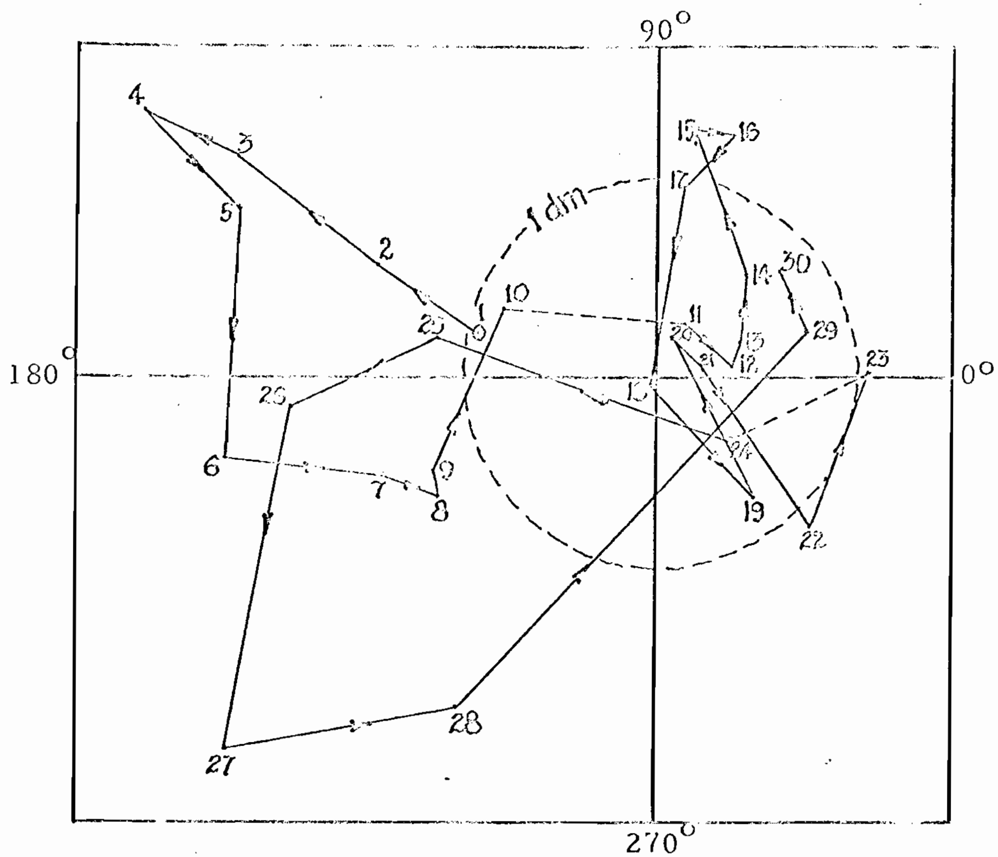

Figure 4c. A polar diagram for harmonic (2, 7). It illustrates mainly progressive (anticlockwise) cycles of motion, similar to component (1, 8).

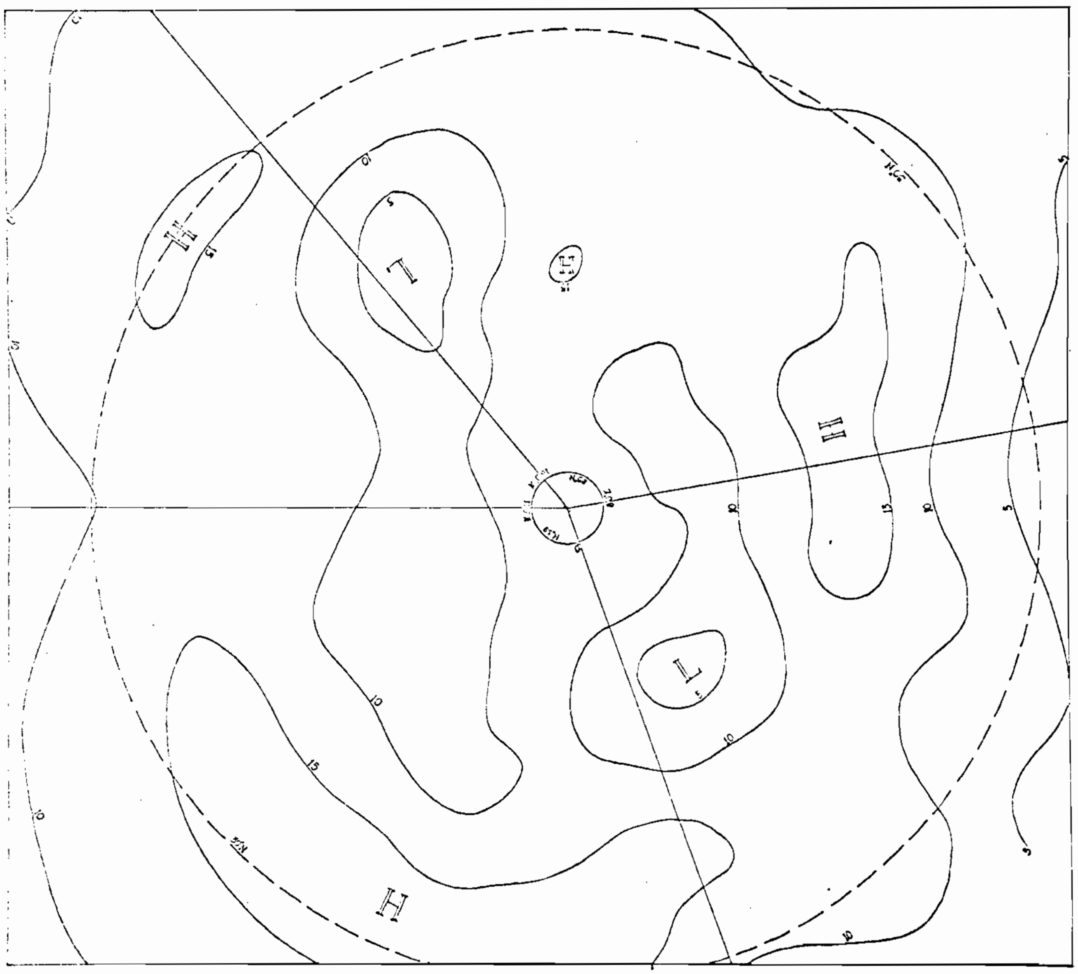

Figure 5a. Mean map of the 1000 mb height field in dm for September 1957 as represented by spherical harmonic analysis. The analysis contains the terms for which $0 \leq m \leq 15$ and $m \leq n \leq 15$.

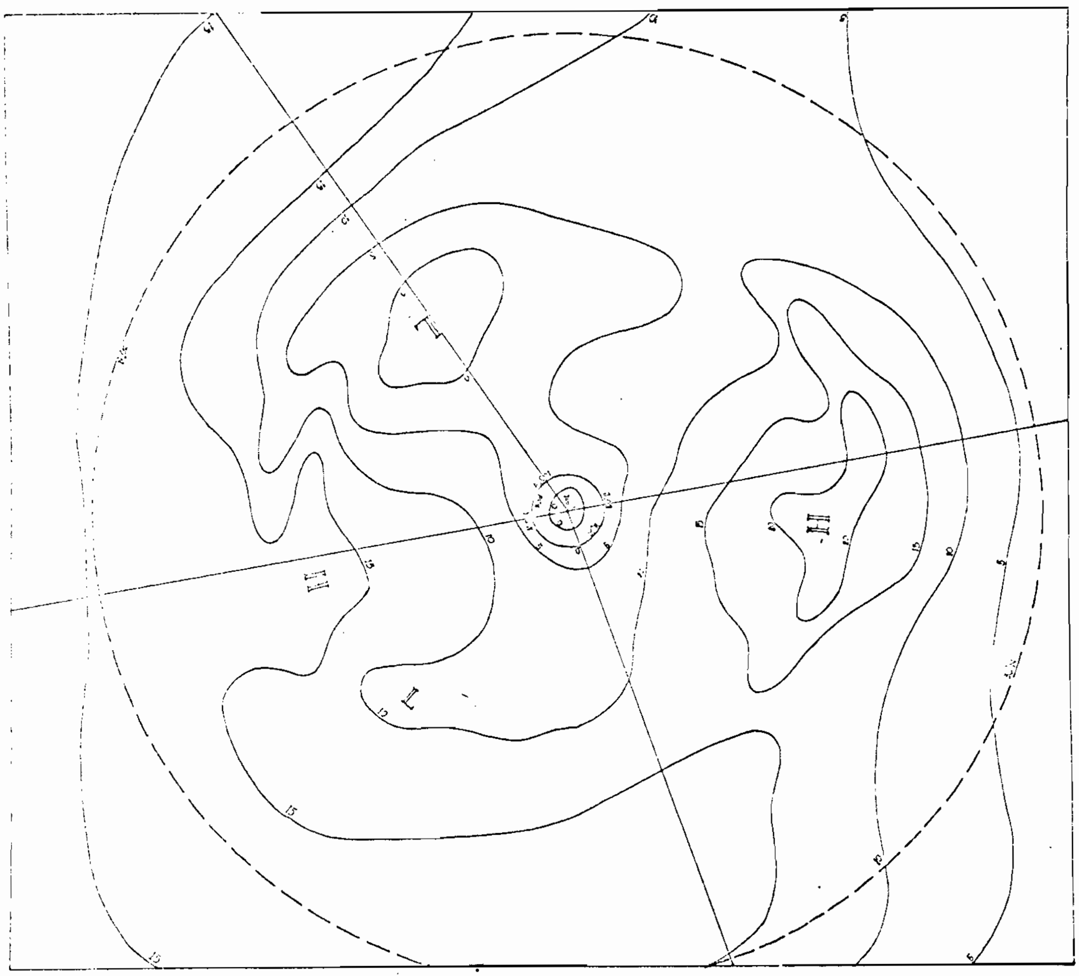

Figure 5b. Height distribution in dm at 1000 mb level for September 1st, 1957 as represented by the ultra long waves in a spherical harmonic analysis. The analysis contains the terms for which $0 \leq m \leq 4$, $m \leq n \leq 10$.

TESSERAL HARMONICS

An immediate picture of the variation with time for the different components is obtained by plotting the variance and phase angle as a function of time. For the components with $m = 1$ and $n=1, 2, 3, 4$ in Figures 6a), b), c) and d), it is seen that a strong stationary component exists; the waves show in general more pronounced progressive motion for larger n indices. For example, wave (1, 1) is located at the end of the month 12 degrees east of its position at the beginning of the month, while wave (1, 4) illustrates a continuous slow progressive motion reaching on the 26th day a position which is about 50 degrees east of its location at the beginning of the month. In some cases, the displacement during one day is relatively large but this always coincides with a small value of the amplitude. Figures 6e) and f) for $(m, n) = (1, 5)$ and (1, 6) respectively are difficult to analyze since the variance for most of the days is below or close to the noise level. However, when the variance has physical significance, these two components also illustrate progressive motion. The graphs in figure 6 also illustrate the large variations in the variance from day to day and from component to component.

Steinberg has presented in his paper, similar graphs for the same components at the 500 mb level for September 1957. It would be interesting to study some aspects of the vertical structure of these waves on the basis of the 1000 mb and 500 mb levels. Harmonic (m, n) = (1, 1) illustrates for the 500 mb and 1000 mb levels, mean positions of 300^{o} and 315^{o} respectively, resulting in an eastward slope of 15^{o}longitude. For (m, n) = (1, 4), the mean positions at the 1000 mb and 500 mb levels are about 43 and 30 degrees longitude, indicating a westward slope of about 13 degrees longitude. Especially for these two components the daily fluctuations of the variance and position are remarkably in phase at the two pressure levels. The variance of (m, n) = (1, 1) at 1000 mb seems to be of slightly larger magnitude than that at 500 mb for the first half of the month, but is generally smaller for the second half of the month. In the case of (m, n) = (1, 4), the variance at 500 mb is always larger than that at 1000 mb and for the first 5 days the ratio is about 2 to 1.

A description of the harmonics (m, n) = (1, 2), (1, 3), (1, 5) and (1, 6) is based on a smaller sample of days due to the small values of the variance at the 1000 mb surface. Thus, when the variance may be considered physically real, components (1, 3) and (1, 6) seem to slope generally westward with height, excepting the days 11 to 16 when (1, 3) illustrates an eastward slope. No simple description can be given to the slopes of components with (m, n) = (1, 2) and (1, 5).

The description of Figure 6, indicates that components (1, 1) and (1, 4) always slope slightly eastward and westward respectively, while the other components have no preferred direction of the vertical slope. This may suggest that either these waves do not necessarily have the same direction of vertical tilt, or since their slopes are small, they may, for climatological purposes be considered to have no change of position with height.

We have seen in table 5 and figure 2b) that the components with (m, n) = (4, n) have a relatively large mean monthly variance. It would thus be useful to consider the daily fluctuations and variance of these tesseral harmonics. These are plotted in figures 7a), b), c), d), e) and f) for the 1000 mb and 500 mb levels.

The waves show, in general, motion towards the east, especially harmonic (4, 7) which contains large magnitude of the variance most of the days. Component (4, 5) shows almost no tilt in the vertical, but (4, 7) clearly illustrates a westward slope which varies between 5 to 8 degrees of longitude. Components (4, 8) and (4, 6) show, where comparison is physically real, a small westward slope. Finally, component (4, 4) is seen to be mainly in the noise level.

The daily variations of the variance at the two levels are remarkably in phase for component (4, 7) and to a less extent for (m, n) = (4, 8), but almost consistently out of phase for (m, n) = (4, 5). We also see that except for (4, 4) and (4, 5), all components amplify with height. The amplification ratio is greater for the even component (4, 6) and (4, 8) than for the odd ones.

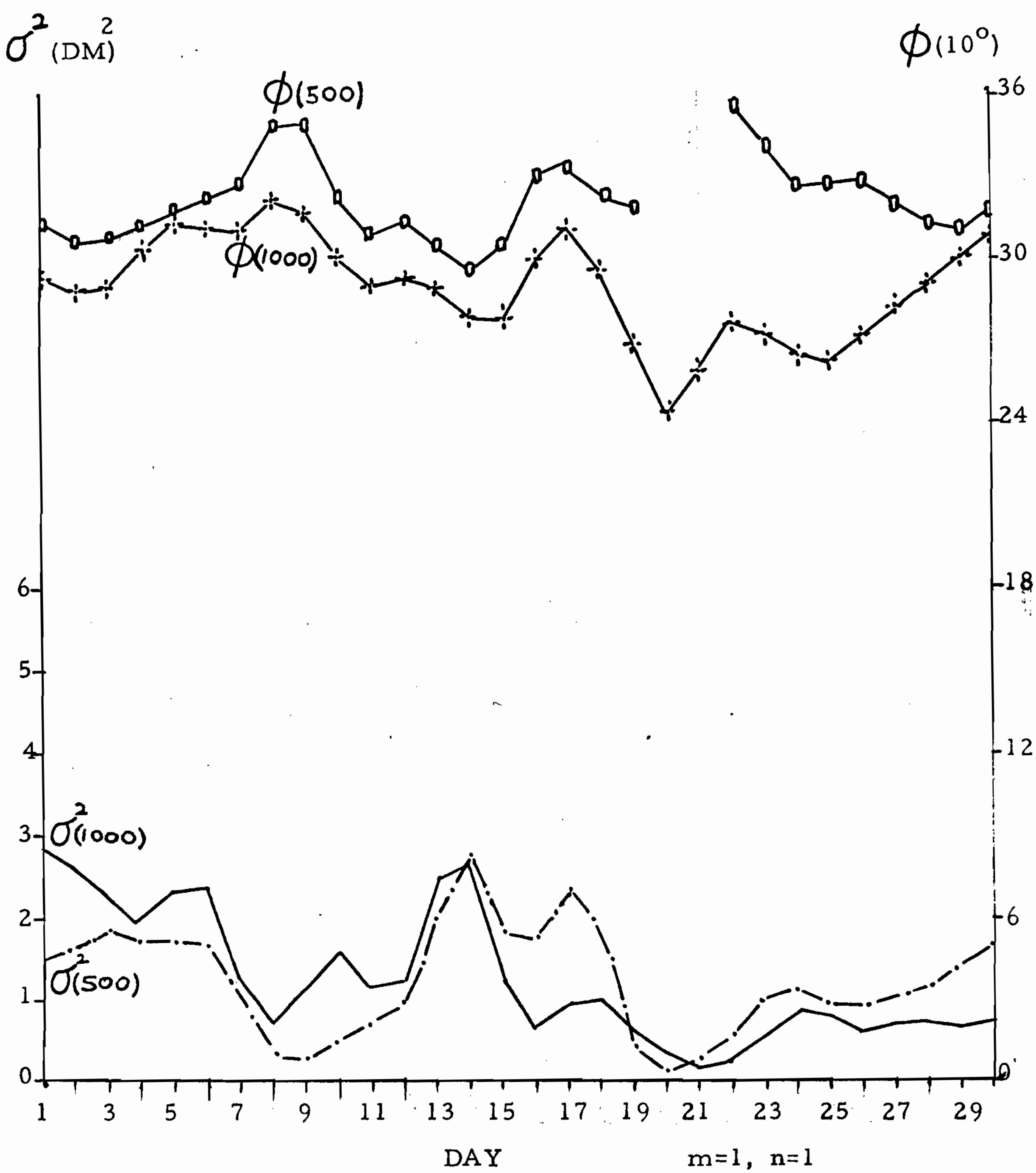

Figure 6a. Successive daily values of the phase angle ϕ and variance σ^2 at the 500 mb (After L. Steinberg) and at the 1000 mb levels for component (m, n)=(1, 1). Non-significant values of the phase angle may be omitted.

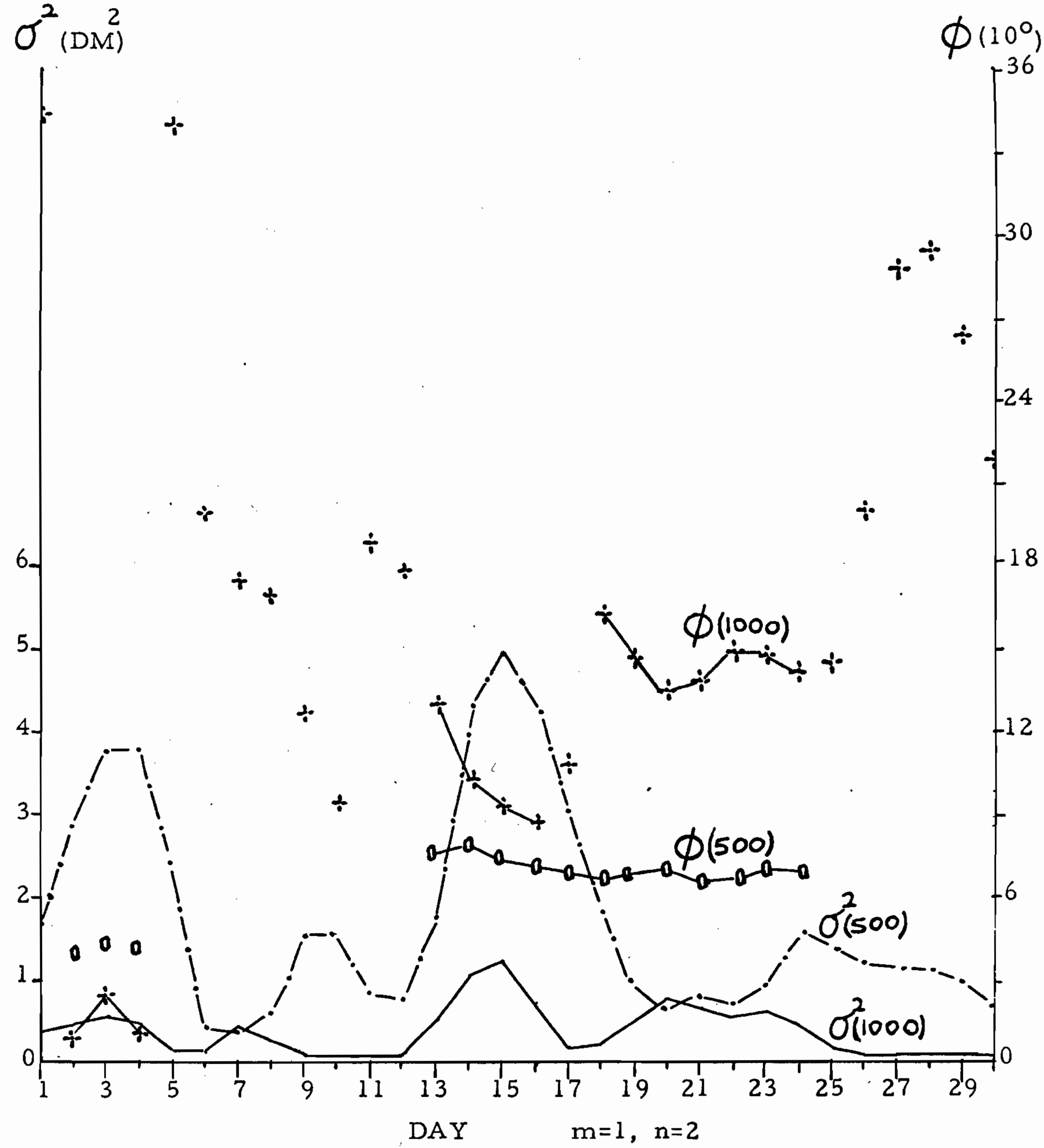

Figure 6b. Successive daily values of the phase angle ϕ and the variance σ^2 at the 500 mb (After L. Steinberg) and at the 1000 mb levels for component (m, n)=(1, 2). Non-significant values of the phase angle may be omitted.

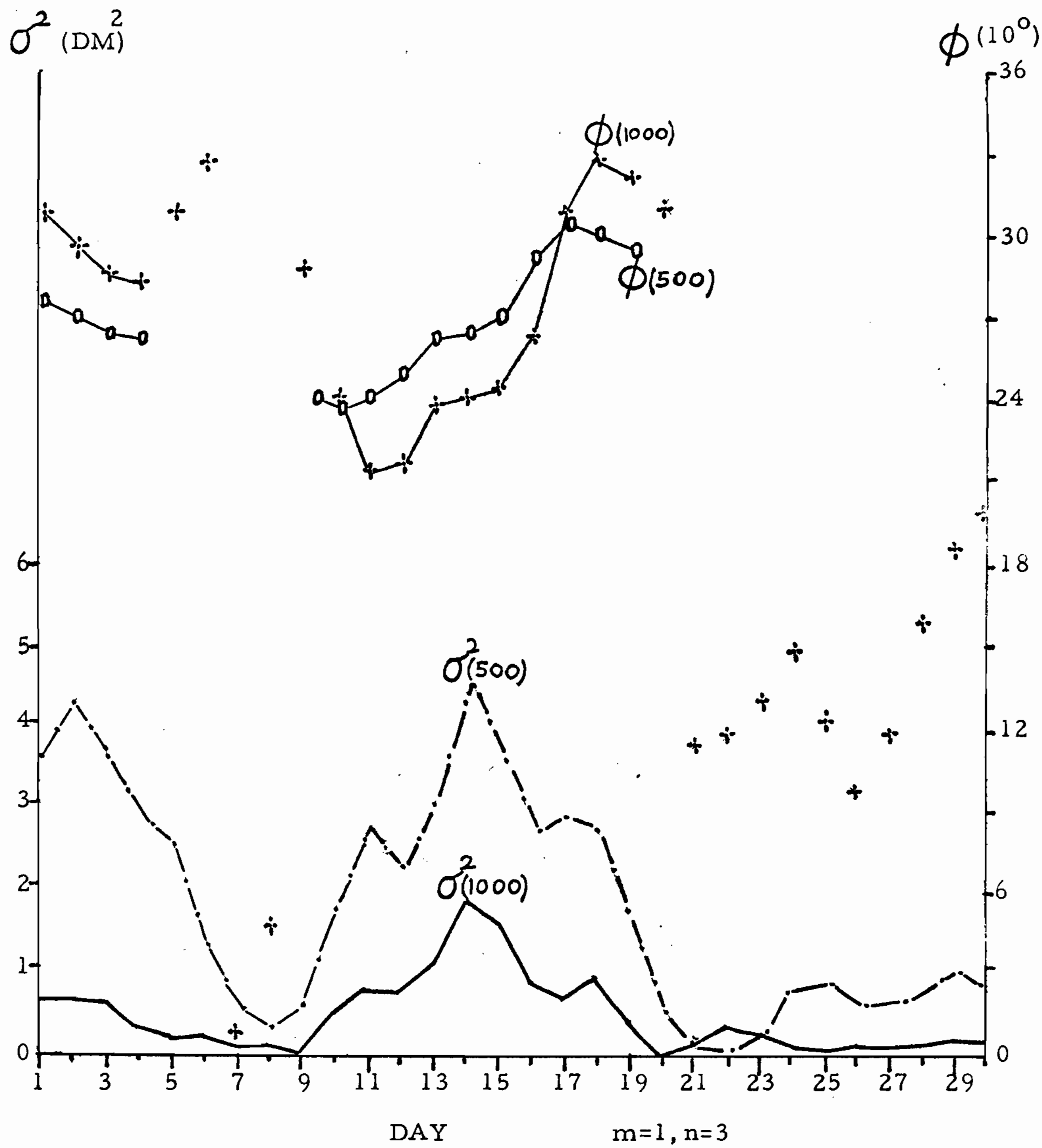

Figure 6c. Successive daily values of the phase angle ϕ and the variance σ^2 at the 500 mb (After L. Steinberg) and at the 1000 mb levels for component (m, n)=(1, 3). Non-significant values of the phase angle may be omitted.

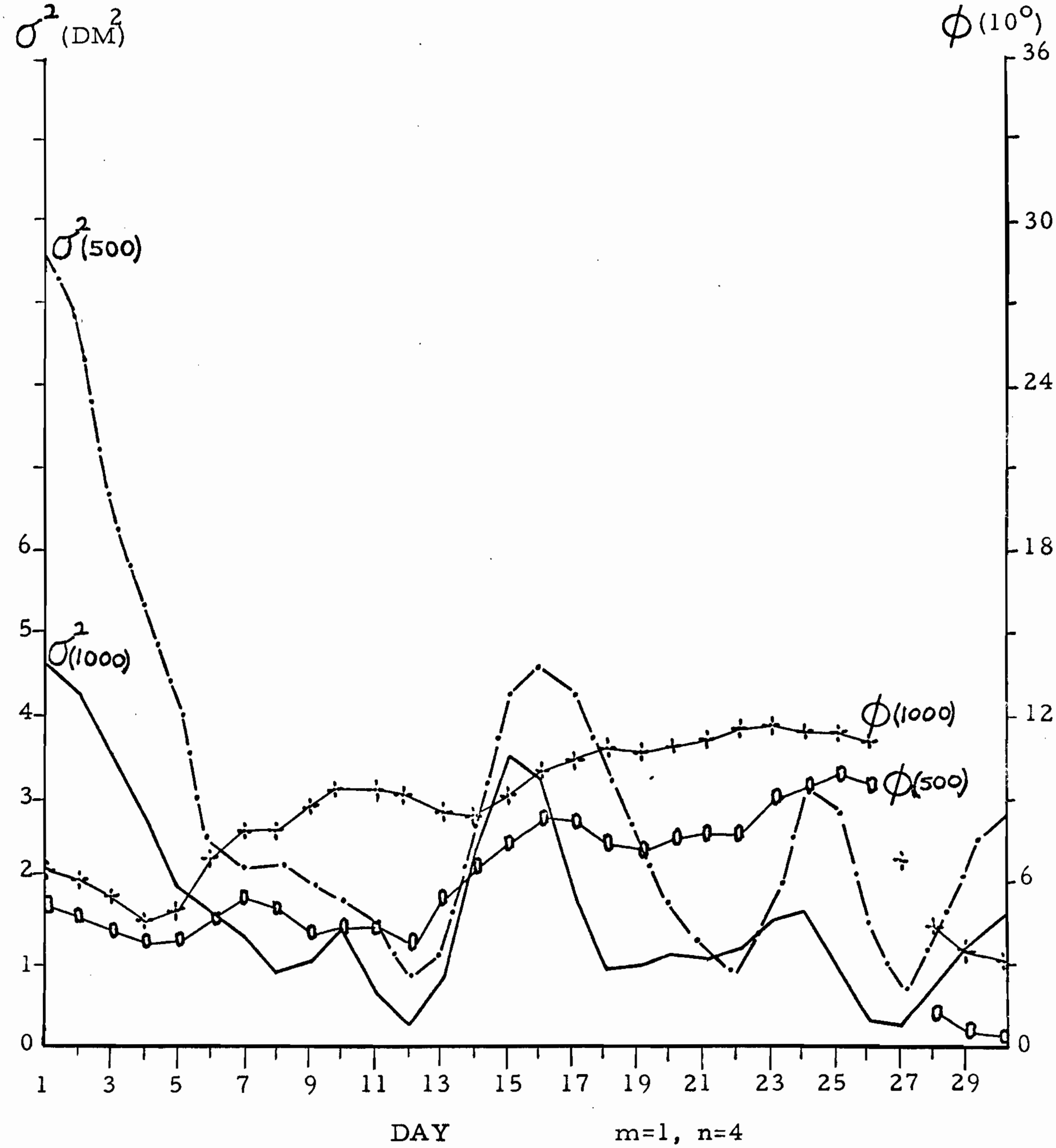

Figure 6d. Successive daily values of the phase angle ϕ and the variance σ^2 at the 500 mb (After L. Steinberg) and at the 1000 mb levels for component (m, n)=(1, 4). Non-significant values of the phase angle may be omitted.

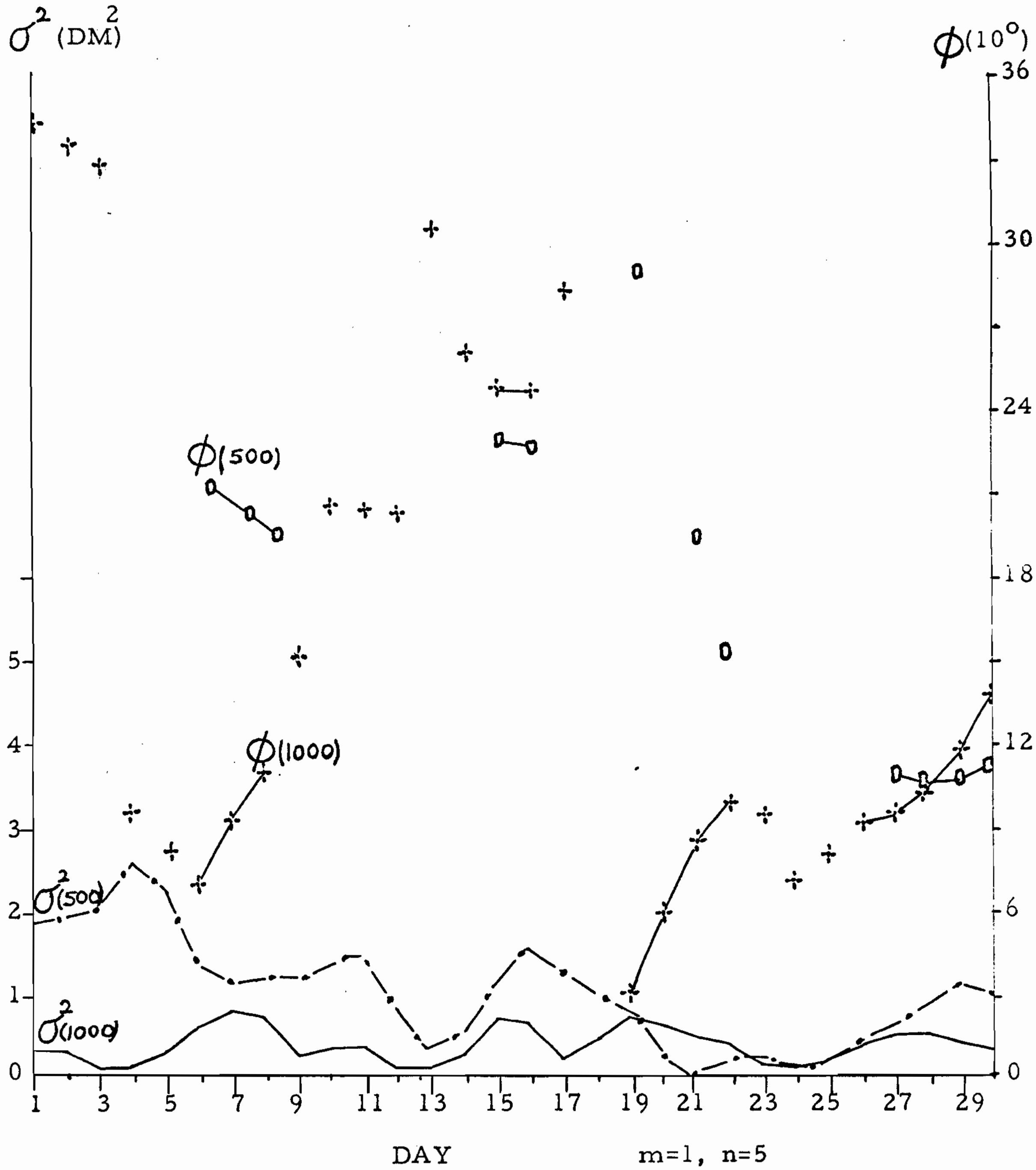

Figure 6e. Successive daily values of the phase angle ϕ and the variance σ^2 at the 500 mb (After L. Steinberg) and at the 1000 mb levels for component (m, n)=(1, 5). Non-significant values of the phase angle may be omitted.

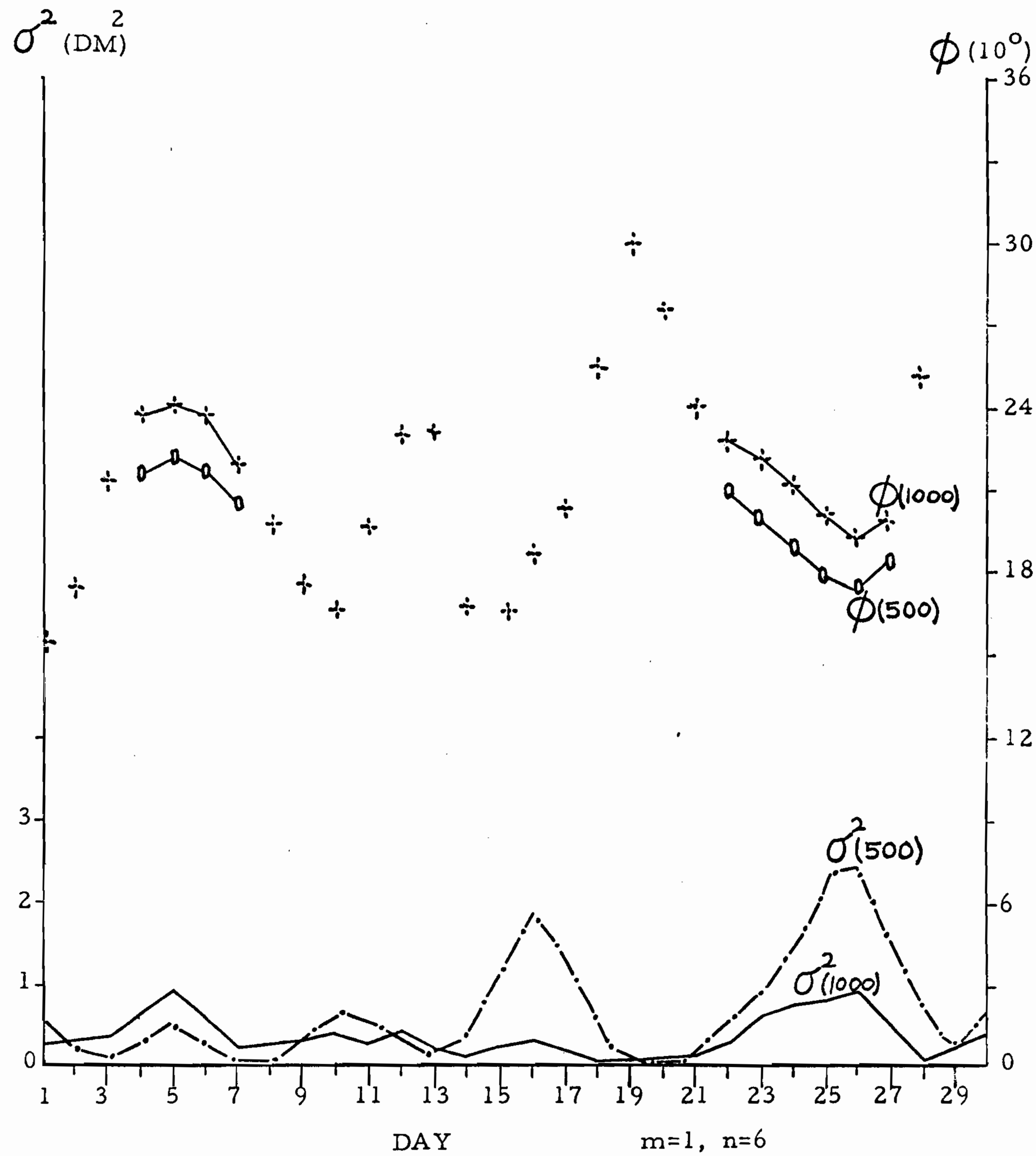

Figure 6f. Successive daily values of the phase angle ϕ and the variance σ^2 at the 500 mb (After L. Steinberg) and at the 1000 mb levels for component (m, n)=(1, 6). Non-significant values of the phase angle may be omitted.

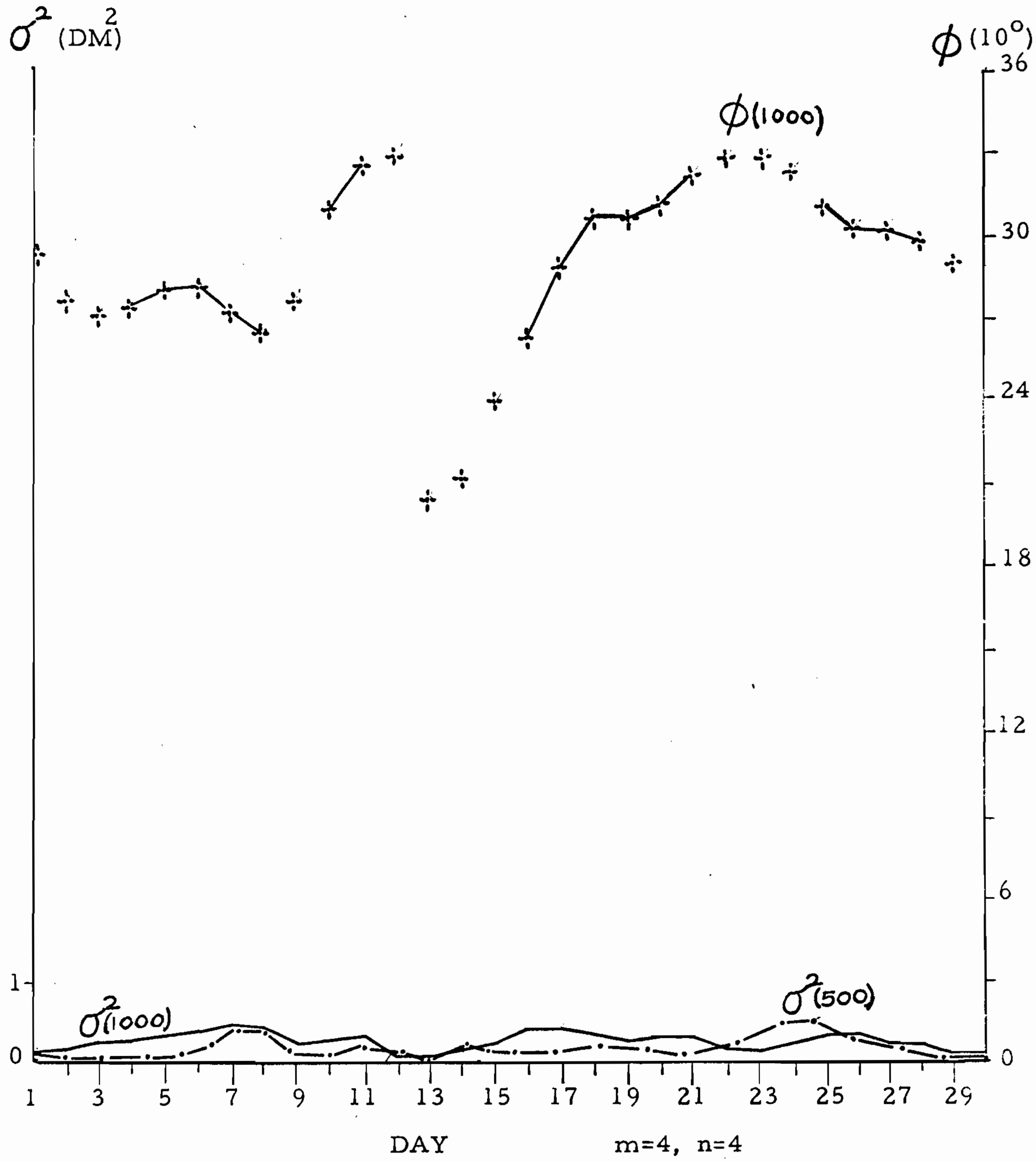

Figure 7a. Successive daily values of the phase angle ϕ and the variance σ^2 at the 500 mb (After L. Steinberg) and at the 1000 mb levels for component (m, n)=(4, 4). Non-significant values of the phase angle may be omitted.

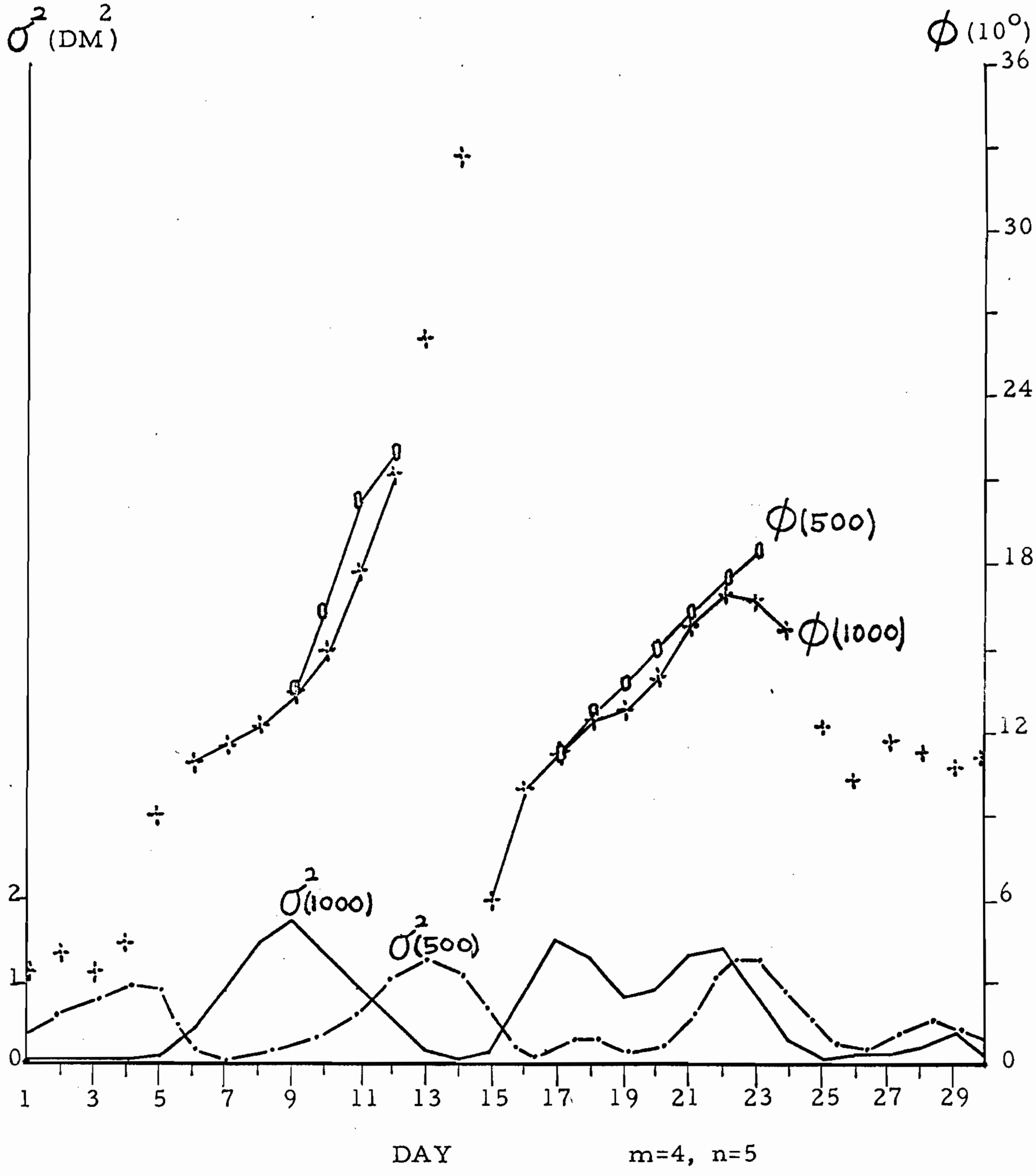

Figure 7b. Successive daily values of the phase angle ϕ and the variance σ^2 at the 500 mb (After L. Steinberg) and at the 1000 mb levels for component (m, n)=(4, 5). Non-significant values of the phase angle may be omitted.

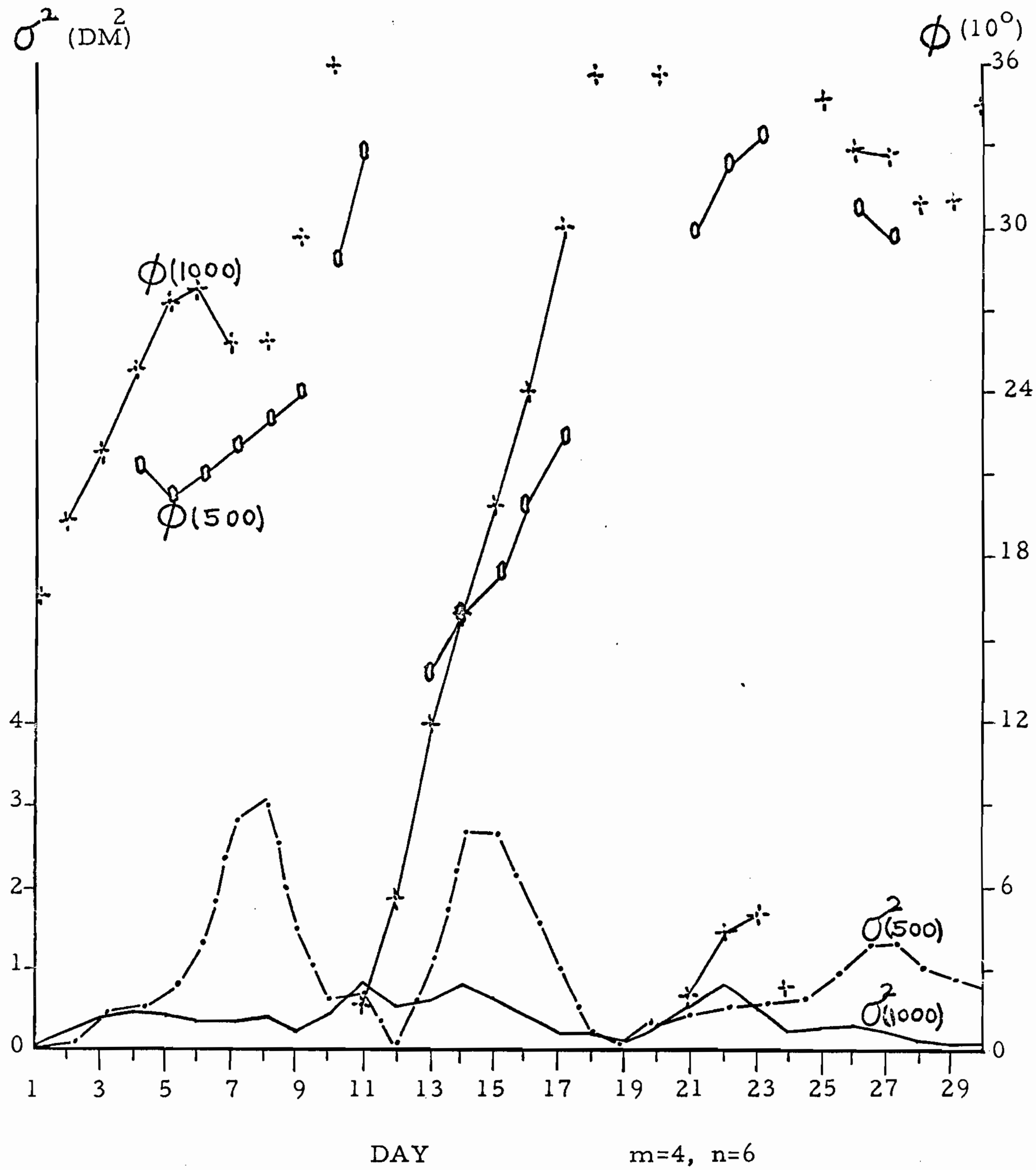

Figure 7c. Successive daily values of the phase angle ϕ and the variance σ^2 at the 500 mb (After L. Steinberg) and at the 1000 mb levels for component (m, n)=(4, 6). Non-Significant values of the phase angle may be omitted.

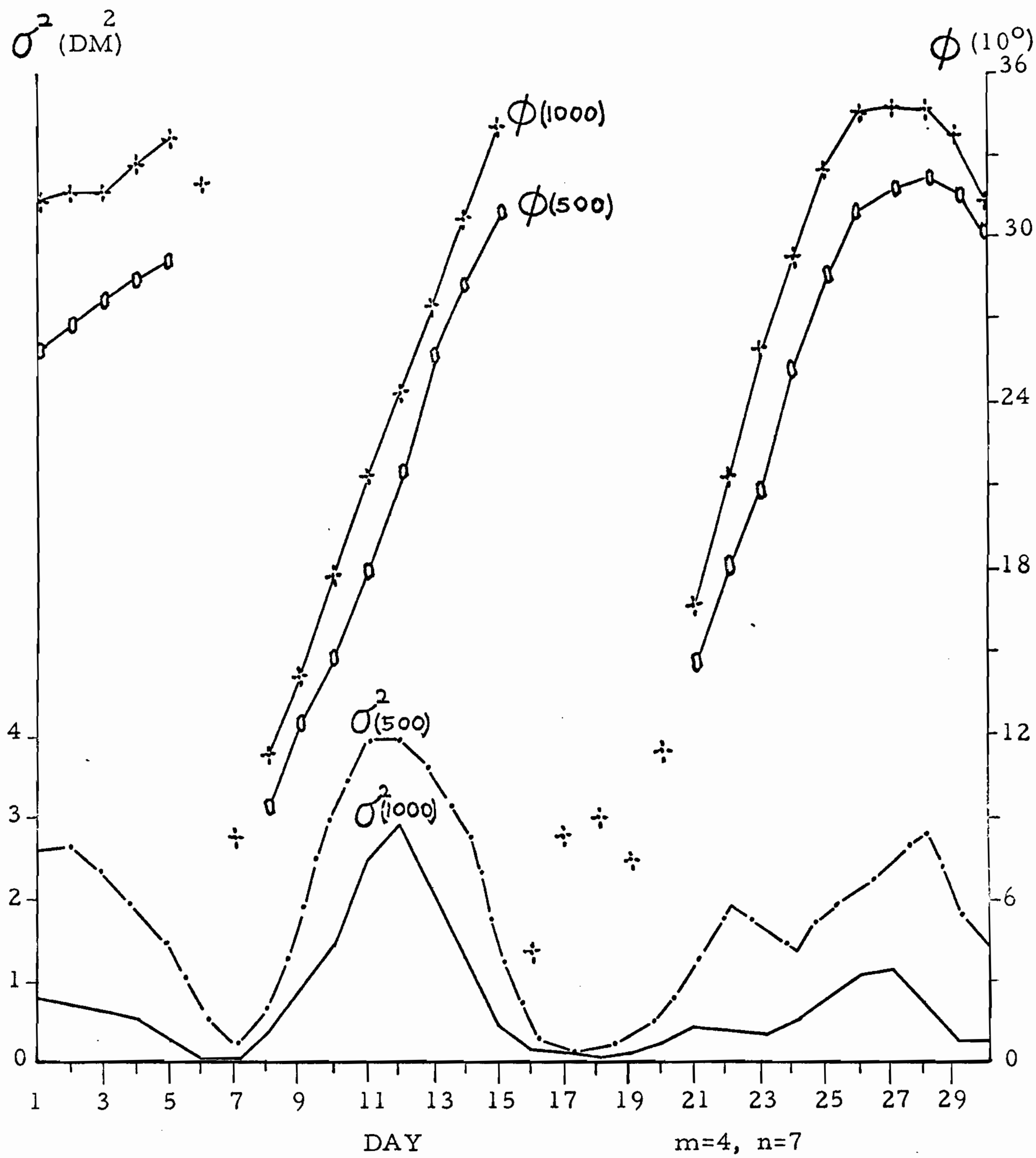

Figure 7d. Successive daily values of the phase angle ϕ and the variance σ^2 at the 500 mb (After L. Steinberg) and at the 1000 mb levels for component (m, n)=(4, 7). Non-significant values of the phase angle may be omitted.

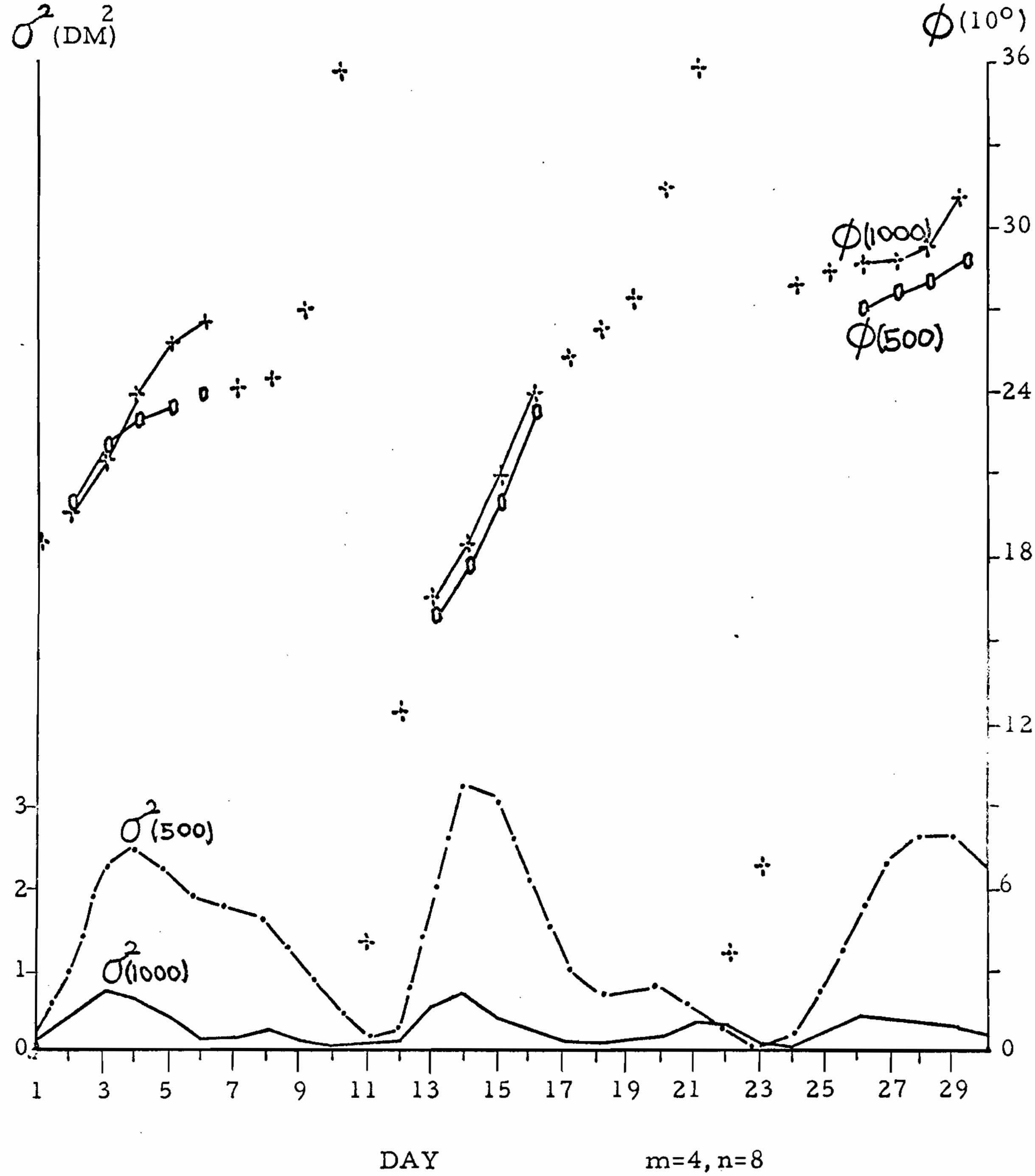

Figure 7e. Successive daily values of the phase angle ϕ and the variance σ^2 at the 500 mb (After L. Steinberg) and at the 1000 mb levels for component (m, n)=(4, 8). Non-significant values of the phase angle may be omitted.

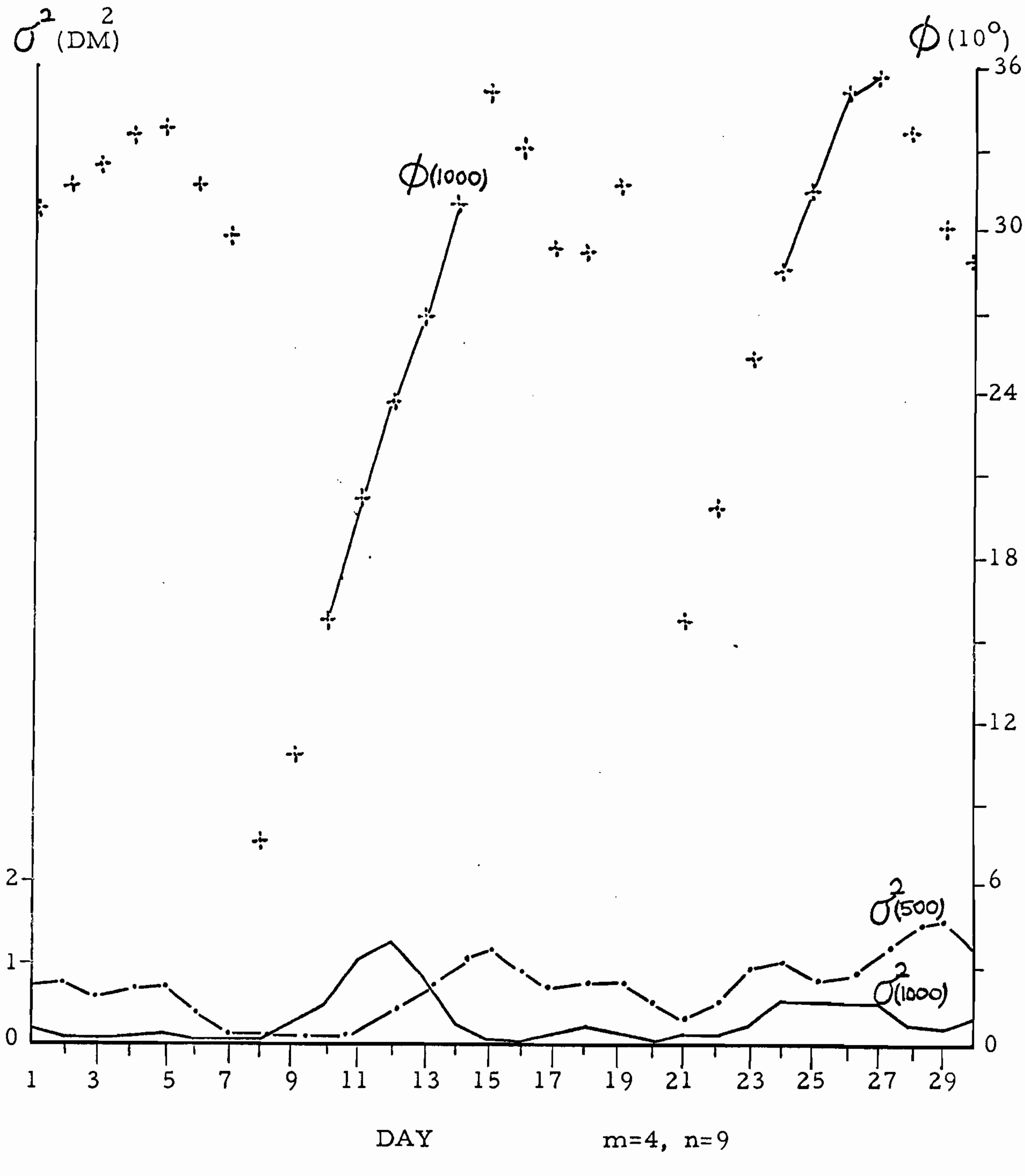

Figure 7f. Successive daily values of the variance σ^2 at the 500 mb (After L. Steinberg) and at the 1000 mb levels and the phase angle at the 1000 mb level for component (m, n)=(4, 9).

ZONAL HARMONICS

The geostrophic zonal flow is described by the zonal components. These terms are found to account for most of the height variance (60 percent of the total variance as indicated in table 6), a fact which indicates that the latitude is the dominant factor in the height-field distribution. In this section of the study, the daily fluctuations in the variance of the major components (0, 1), (0, 2), (0, 3) and (0, 4) are discussed.

Since most of the àtmosphere lies above the 1000 mb pressure level,and its mass remains constant with time, it follows that the area weighted mean height of the global 1000 mb surface varies very slightly with time. Figure 8 shows that component (0, 0), which is the area weighted mean height, is essentially constant with time; the mean height is about 14 decameters.

In table 6 we find that the sum of the mean monthly variance of the odd components (0, 1) and (0, 3) and that of the even components (0, 2) and (0, 4) contain about 26 percent and 25 percent of the total variance, respectively. Thus, these odd and even harmonics contribute about equally, in the mean, to the total height field. However, figures 9a) and b) show that the even and odd components alternate in cycles of predominance during the month. Harmonics (0, 2) and (0, 4) dominate during the first 14 days, while (0, 1) and mainly (0, 3) dominate during the next 10 days.

During the last 6 days, the even components begin to dominate again. Thus, there are fluctuations in the symmetry of the meridional height profile, with respect to the equater.

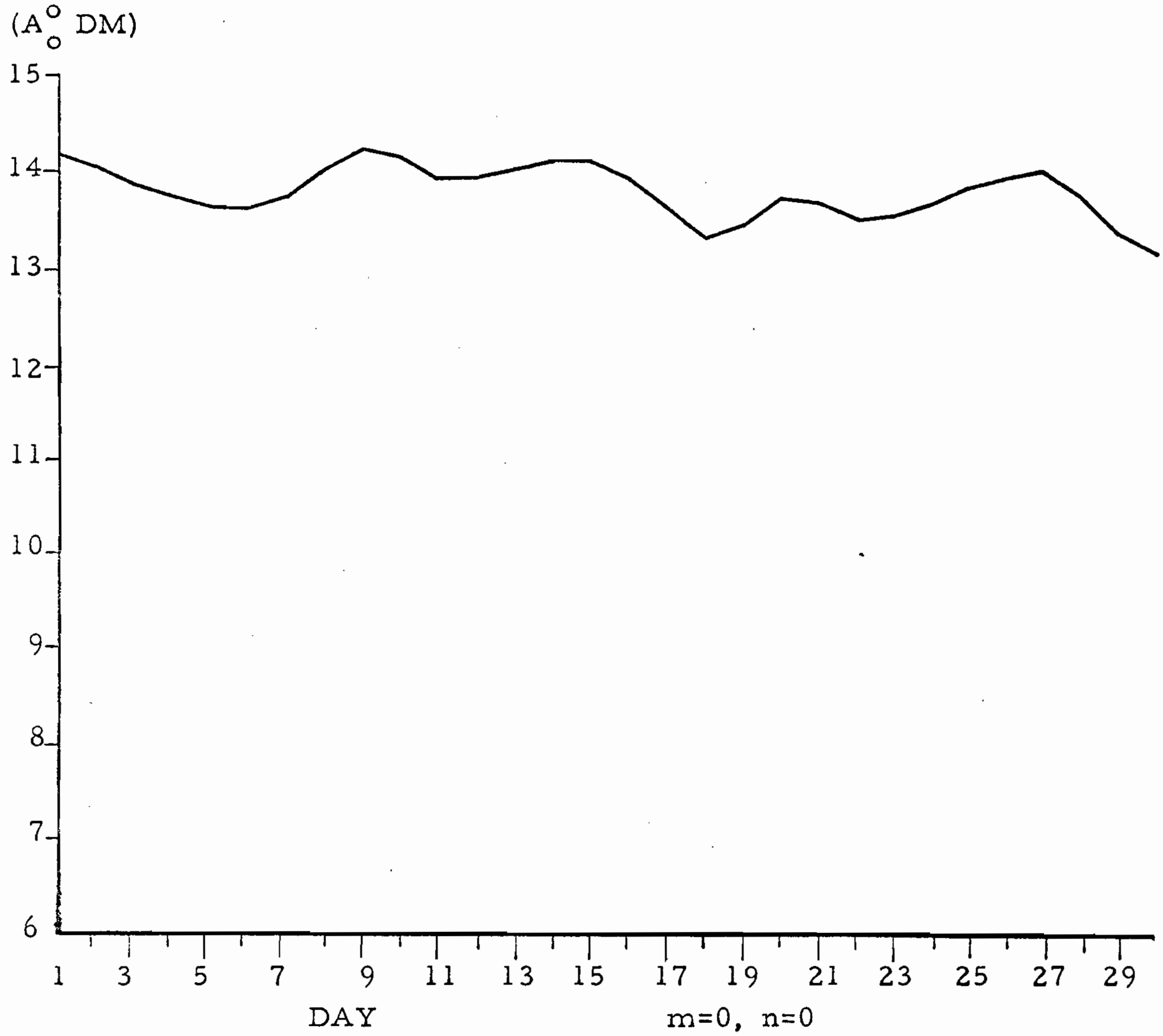

Figure 8. Daily values of A_o^o, which are directly proportional to the area weighted mean height of the global 1000 mb surface. The constant of proportionality is $P_o^o = \frac{1}{\sqrt{2}}$

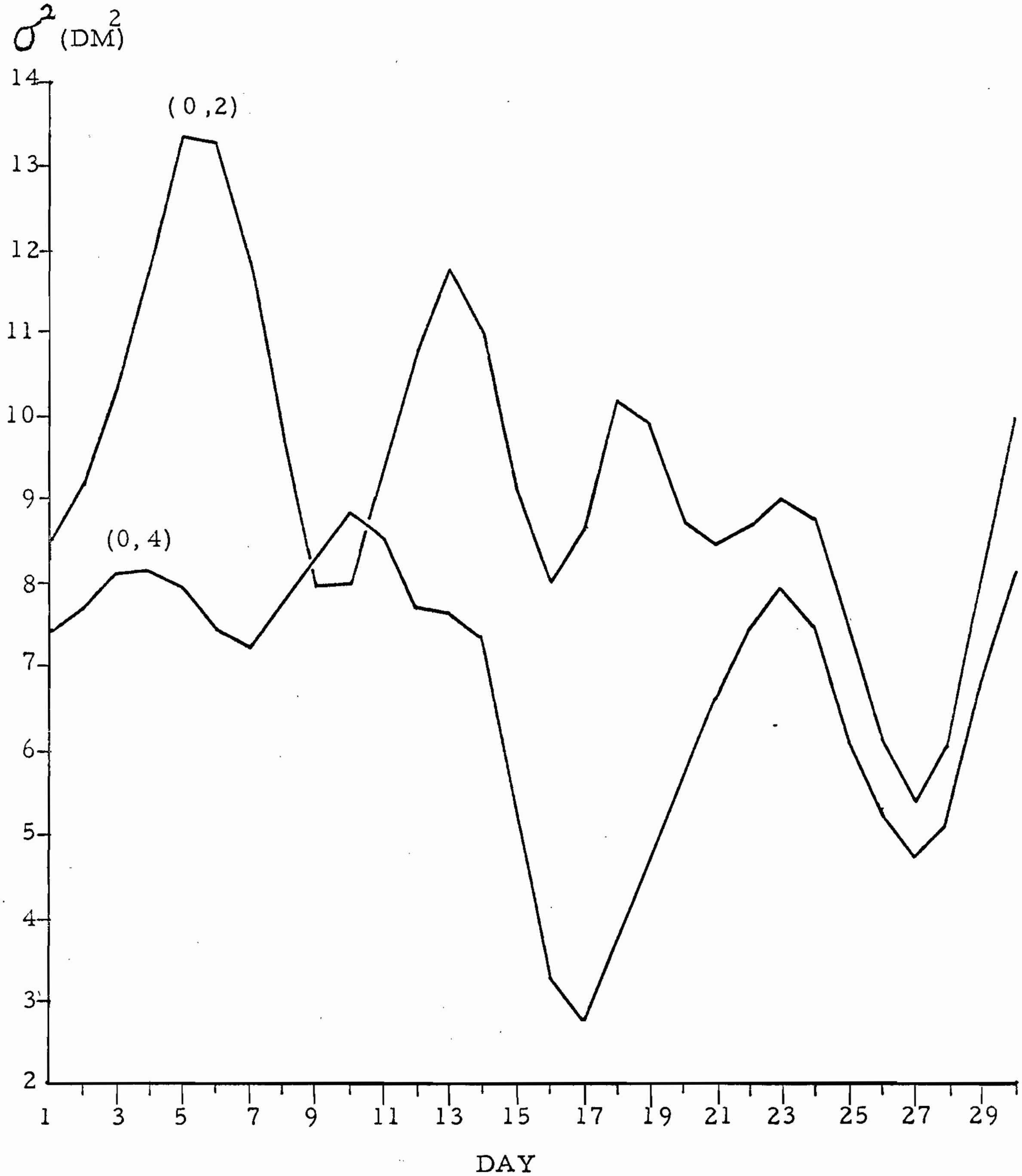

Figure 9a. Successive daily values of the variance σ^2 of the zonal components (0, 2) and (0, 4) at the 1000 mb level. The sum of their variance reaches high values during the first 6 days and last few days of the month.

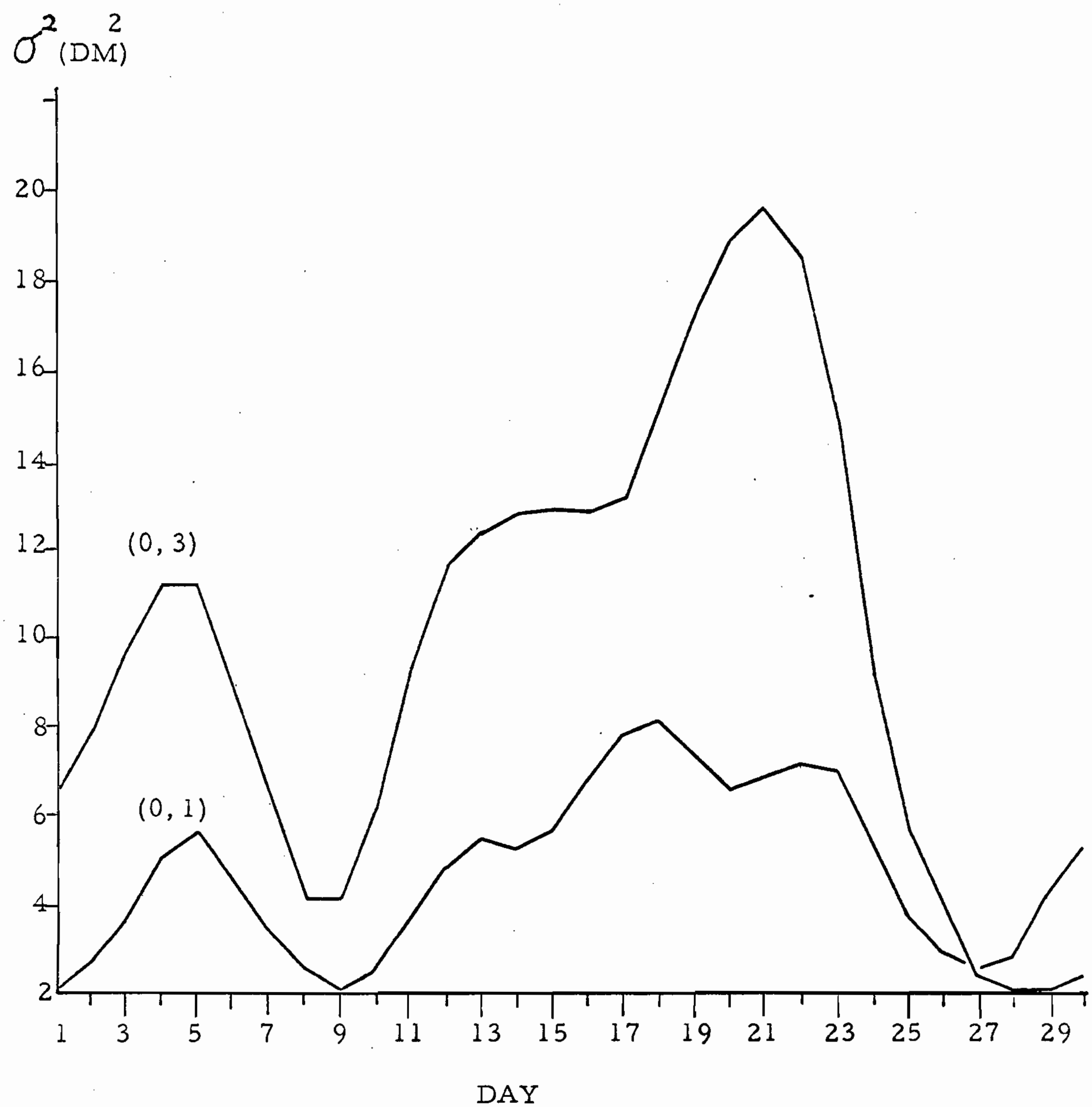

Figure 9b. Successive daily values of the variance σ^2 of the zonal components (0, 1) and (0, 3) at the 1000 mb level. The sum of their variance reaches high values between the 18th and 23rd days of the month.

MEAN TEMPERATURE OF THE LOWER TROPOSPHERE

Since spherical harmonic coefficients of the height field at the 500 mb level (Steinberg) and those of the 1000 mb level are available, it is a simple procedure, through the Hypsometric Equation, to obtain the spherical harmonic coefficients of the mean temperature between these two pressure levels. This would permit some investigations about the lower tropospheric temperature field.

Figures 10a) and b) illustrate that harmonic (0, 1) is becoming less dominant with time, while the variance of (0, 2) increases during the month. We also note that (0, 2) contributes to the temperature field more than (0, 1) all through the month. This indicates that although the meridional temperature profile was largely symmetrical with respect to the equator during September 1957, its symmetry increased during the 30 days. These two zonal components describe most of the temperature field.

Figures 11a), b) and c) are also presented to illustrate that the tesseral harmonics of the lower tropospheric temperature field indicate generally very small values of the variance. Hence, the temperature field is mainly a function of latitude.

Finally figure 12 illustrates that the first component of the spherical harmonic series, i.e. the area weighted global mean temperature of the lower troposphere, to be about 2.2°C during September 1957.

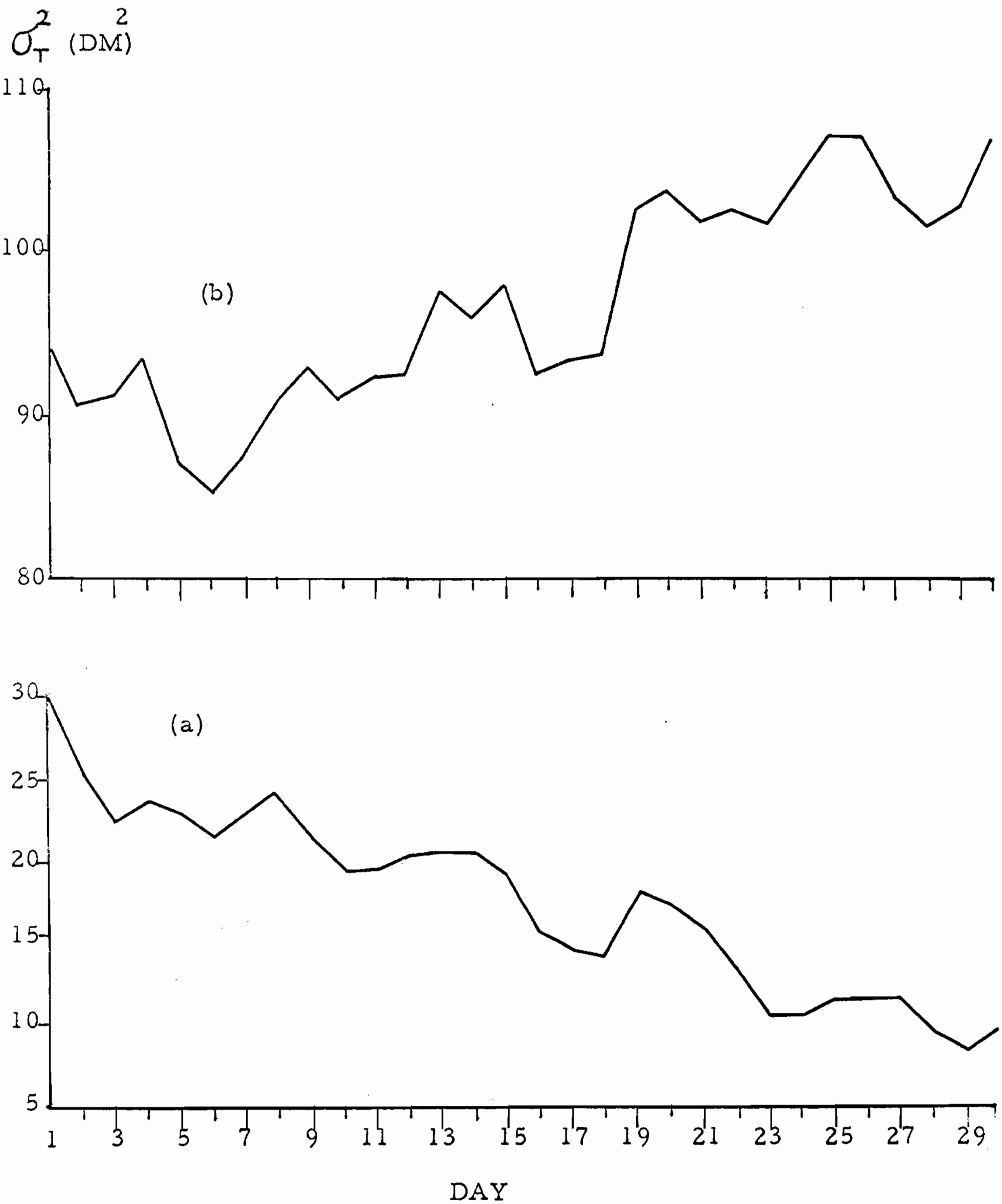

Figure 10. Successive daily values of the variance σ_T^2 (of the lower tropospheric temperature field) of the zonal components (0, 1) and (0, 2).

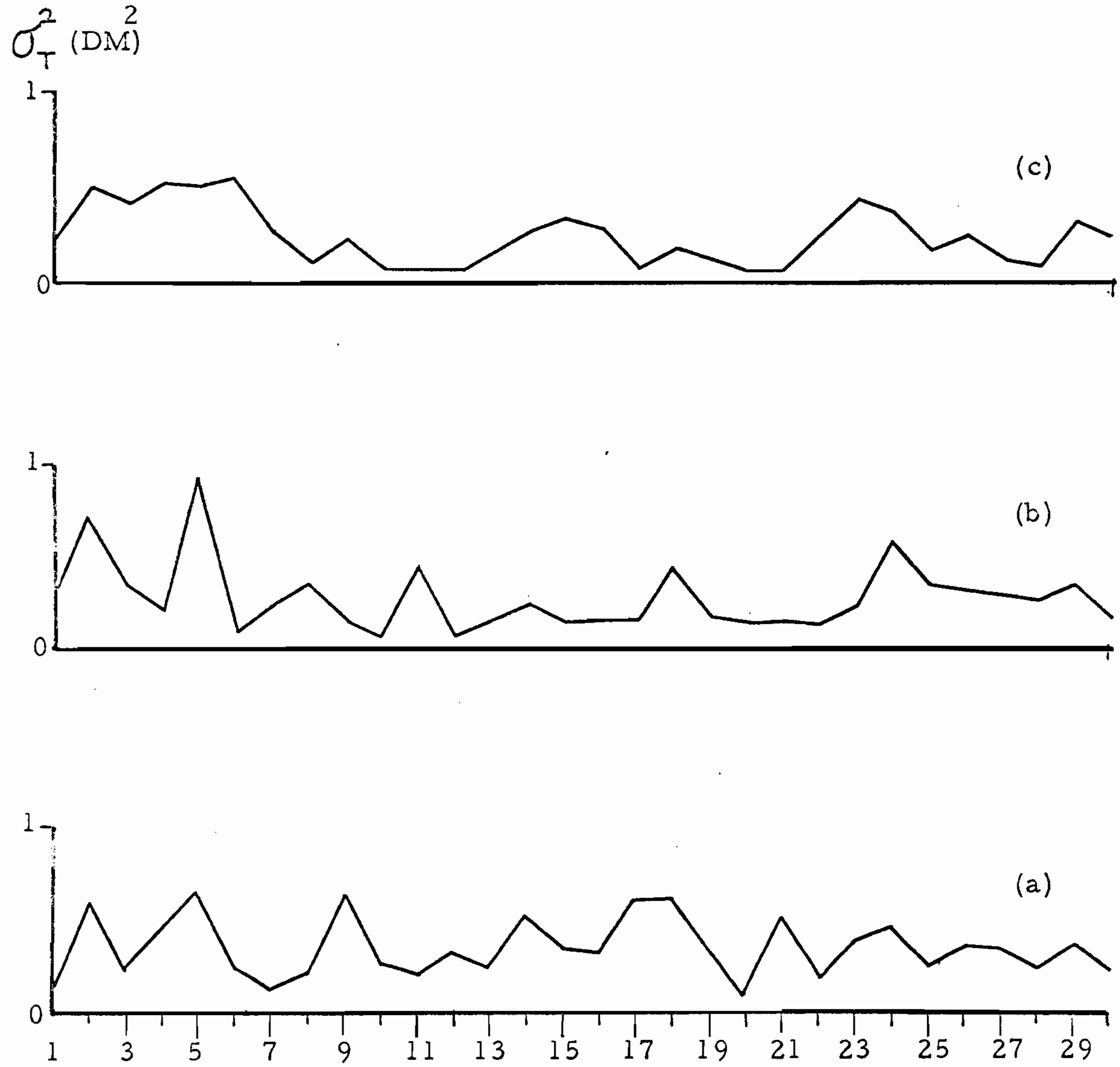

Figure 11. Successive daily values of the variance σ_T^2 (of the lower tropospheric temperature field) of the components (1,2), (1,3) and (2,4).

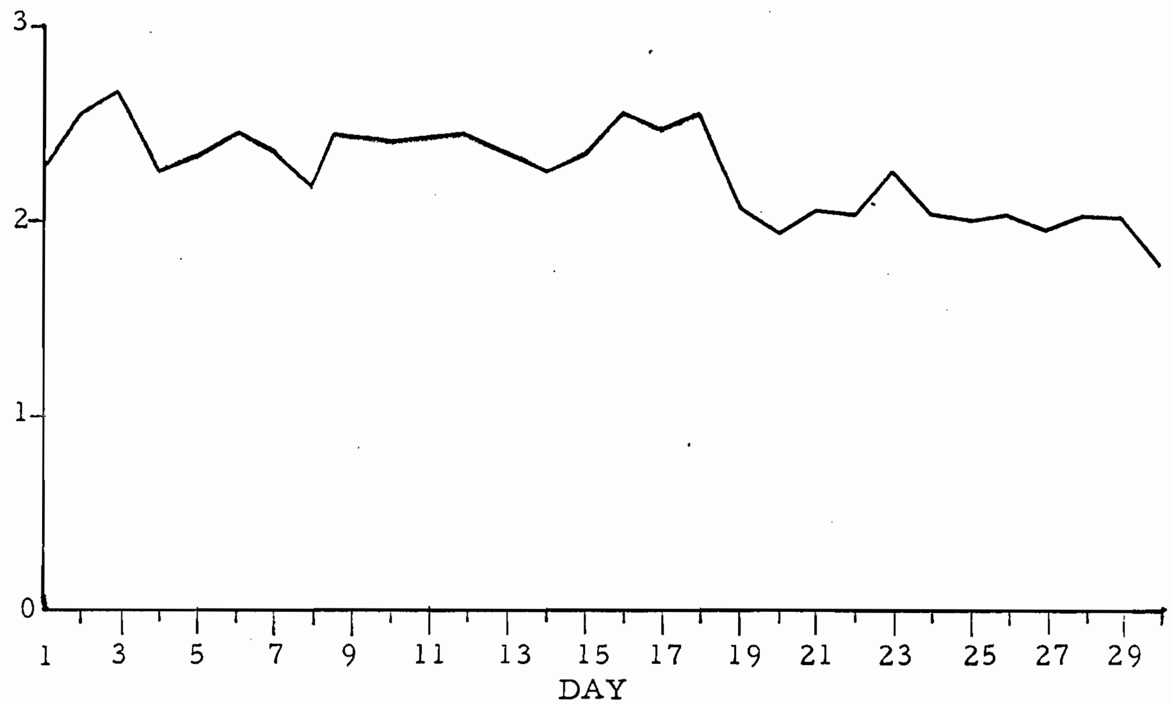

Figure 12. Daily values of the area weighted mean temperature of the global lower troposphere for September 1957.

SUMMARY AND CONCLUSIONS

The present study analyzed the height field of the global 1000 mb surface on a daily basis for September 1957 in terms of spherical harmonics. The main topics reviewed in the work are:

(1) three possible methods of numerical integration

(2) the variance contributions of the major components

(3) the vertical structure of some tesseral harmonics on the basis of the 1000 mb and 500 mb pressure levels

(4) the zonal harmonics

and (5) the temperature field of the lower troposphere

Examination of these aspects led to the following conclusions:

1. Integration of the spherical harmonic coefficients by Simpson's rule proved to be quite accurate for the zonal components, while the Trapezoidal rule was found to be better for the wave components. The Gaussian method was found to be superior to the Trapezoidal rule but inferior to Simpson's rule for the zonal harmonics.

2. Variance Analysis:

(i) The zonal harmonics contain about 60 percent of the total variance of the height field, while the wave components with m=1, 2, 3, 4 contain about 31 percent. Among the wave components, the ones with three nodes in the North-South direction (n-m=3) contained most of the variance.

(ii) The study of the motion of planetary waves shows their dependence on the latitudinal (represented by n-m or n) as well as the longitudinal (represented by m) scale. It follows that any discussion of planetary waves must also take the latitudinal dependence into account.

3. Vertical Structure:

(i) Some of the long waves slope eastward, some westward and others change slope with time. Hence, no one direction of the vertical slope is likely to apply to all the long waves.

(ii) Most of the analyzed waves show increase of amplitude with height. Notable exceptions are the sectorial harmonics (1, 1) and (1, 4).

4. The meridional height field for September 1957 alternates in its symmetry with respect to the equator. It thus appears that the odd and even zonal harmonics are both significant during September.

5. The temperature field of the lower troposphere is mainly dependent on latitude and to a much less extent on longitude.

REFERENCES

CHAPMAN, S., and BARTELS, J., 1940: "Geomagnetism", vol.II, Oxford Univ. Press, Chap. XVII

CRAIG, R.A., 1945: "A solution of the nonlinear vorticity equation for atmospheric motion", J. Meteor., 2 pp. 175-178

DELAND, R.J., 1965: "Some observations of the behaviour of spherical harmonic waves, Monthly Weather Review, vol. 93, No. 5, pp.307-312

DELAND, R.J., 1965: "On the scale analysis of travelling planetary waves", Tellus vol.17, pp. 527-528

ELIASSEN, E., and MACHENHAUER, B., 1965: "A study of the fluctuations of the atmospheric planetary flow patterns represented by spherical harmonics", Tellus, vol.17, pp. 220-38

GILCHRIST, A., 1957: "The representation of circumpolar 500 mb charts by a series of spherical harmonics", British Meteor. Off., Meteor. Res. Pap., No. 1040, 9 pp.

HAURWITZ, B., 1940: "The motion of atmospheric disturbances", J. Marine Res., vol.3, No. 1, pp. 35-50

HAURWITZ, B., 1940: "The motion of atmospheric disturbances on the spherical earth", J. Marine Res., 3 pp. 254-267

HAURWITZ, B., and CRAIG, R.A., 1952: "Atmospheric flow patterns and their representation by spherical surface harmonics", U.S. Air Force, Cambr. Res. Cnt., Geophysics. Res. Pape., No. 14, 78 pp.

STEINBERG, H.L., 1965: "A spherical harmonic specification of the global 500 mb surface", Thesis submitted for the degree of Master of Science, McGill University (unpublished).

Reference Charts

I.G.Y. World Weather Maps, Part I, Northern Hemisphere, Sea Level and 500 mb Charts, issued by U.S. Dept. of Commerce, Sept. 1957.

I.G.Y. World Weather Maps, Part II, Equatorial Region, Sea Level and 500 mb charts, issued by the Federal Republic of Germany, Sept. 1957.

I.G.Y. World Weather Maps, Part III, Southern Hemisphere, Sea Level and 500 mb charts, issued by the Republic of South Africa, Sept. 1957.

Monthly Climate Data For the World, Sponsored by W.M.O. in cooperation with U.S. Weather Bureau, Sept. 1957, vol. 10, No.9.

APPENDIX

Properties of Spherical Harmonics and Their Introduction to Meteorology

Consider Laplace's Equation in spherical polar coordinates,

$$rD_r^2(rV) + \frac{1}{\sin\theta} D_\theta(\sin\theta\, D_\theta V) + \frac{1}{\sin^2\theta} D_\lambda^2 V = 0 \tag{5}$$

where V is a potential function of r, θ, λ, the spherical polar coordinates.

We assume $V(r,\theta,\lambda) = R(r)\,\theta(\theta)\,\lambda(\lambda)$

By substituting (6) into (5), we obtain

$$\frac{r}{R}\frac{d^2(rR)}{dr^2} + \frac{1}{\theta\sin\theta}\frac{d\left(\sin\theta\frac{d\theta}{d\theta}\right)}{d\theta} + \frac{1}{\lambda\sin^2\theta}\frac{d^2\lambda}{d\lambda^2} = 0 \tag{6}$$

i.e.

$$\frac{r}{R}\frac{d^2(rR)}{dr^2} = -\frac{1}{\theta\sin\theta}\frac{d\left(\sin\theta\frac{d\theta}{d\theta}\right)}{d\theta} - \frac{1}{\lambda\sin^2\theta}\frac{d^2\lambda}{d\lambda^2}$$

left hand side is a function of r only and right hand side is a function of λ and θ only, then each side must be equal to a constant, say n(n+1)

$$\frac{r}{R}\frac{d^2(rR)}{dr^2} = -\frac{1}{\theta\sin\theta}\frac{d\left(\sin\theta\frac{d\theta}{d\theta}\right)}{d\theta} - \frac{1}{\lambda\sin^2\theta}\frac{d^2\lambda}{d\lambda^2} = n(n+1)$$

$$\frac{r}{R}\frac{d^2(rR)}{d\,r^2} - n(n+1) = 0 \tag{7}$$

and

$$-\frac{1}{\theta\sin\theta}\frac{d}{d\theta}\sin\theta\frac{d\theta}{d\theta} - \frac{1}{\lambda\sin^2\theta}\frac{d^2\lambda}{d\lambda^2} - n(n+1) = 0$$

$$\frac{\sin\theta}{\theta}\frac{d}{d\theta}\sin\theta\frac{d\theta}{d\theta} + \frac{1}{\lambda}\frac{d^2\lambda}{d\lambda^2} + n(n+1)\sin^2\theta = 0$$

similar to the above argument, we introduce another constant m^2 so that

$$\frac{\sin\theta}{\theta}\frac{d}{d\theta}\sin\theta\frac{d\theta}{d\theta} + n(n+1)\sin^2\theta = -\frac{1}{\lambda}\frac{d^2\lambda}{d\lambda^2} = m^2$$

$$\therefore \quad \frac{d^2\lambda}{d\lambda^2} + m^2\lambda = 0 \tag{8}$$

and

$$\frac{1}{\sin\theta}\frac{d}{d\theta}\sin\theta\frac{d\theta}{d\theta} + \left|n(n+1) - \frac{m^2}{\sin^2\theta}\right|\theta = 0 \tag{9}$$

The general solution of (8) for a fixed m is

$$\lambda(\lambda) = A\cos m\lambda + B\sin m\lambda$$

Equation (9) has for one of its solutions, the associated Legendre Polynomial $P_n^m(\theta)$ given by

$$P_n^m(\theta) = \frac{2n!}{2^n\,n!(n-m)!}\sin^m\theta\Big[\cos^{n-m}\theta - \frac{(n-m)(n-m-1)}{2(2n-1)}\cos^{n-m-2}\theta + \frac{(n-m)(n-m-1)(n-m-2)(n-m-3)}{2\cdot 4(2n-1)(2n-3)}\cos^{n-m-4}\theta + \cdots\cdots\Big] \tag{10}$$

where m is the order and n the degree of the polynomial.

These $P_n^m(\theta)$ are orthogonalized in the following manner

$$\int_{-1}^{+1} P_n^m(u)\,P_{n'}^m(u)\,du = 0 \qquad \text{for} \quad n \neq n'$$

$$= \frac{2}{2n+1}\frac{(n+m)!}{(n-m)!} \qquad \text{for} \quad n = n'$$

Thus to normalize these $P_n^m(\Theta)$, the normality factor to be used must be

$$\sqrt{\frac{2n+1}{2}\,\frac{(n-m)!}{(n+m)!}}$$

Properties of $P_n^m(\Theta)$

In Figure 13 P_7^o, P_7^1, ...P_7^7 are represented as functions of θ. These curves illustrate the following general properties of the Associated Legendre Polynomials,

(a) Every Associated Legendre Polynomial $P_n^m(\theta)$ has n-m real different zeros between $\theta=0$ and $\theta=\pi$. The zonal functions $P_n^o(\theta)$ have the value =1 at the north pole ($\theta=0^o$) and $(-1)^n$ at the south pole ($\theta=\pi$); every other function $P_n^m(\theta)$, $m > 0$, is zero at both poles as well as at (n-m) values of θ between the poles.

(b) According as n-m is even or odd, P_n^m is symmetrical or antisymmetrical with respect to the equator, i.e.

$$P_n^m(\Theta) = (-1)^{(n-m)} P_n^m(\pi - \Theta)$$

When (n-m) is odd, one of the (n-m) zeros of P_n^m occurs at the equator $\theta=\pi/2$

(c) The normalized functions P_n^n which can be given by

$$P_n^m(\ ) = \frac{\sqrt{(2n+1)(2n)!}}{\sqrt{2}\ 2^n\ n!}\sin^n\theta$$

are very small over an extensive region round the poles (see P_7^7 in Fig. 13).

Tesseral and Sectorial Surface Harmonics

The surface harmonics $P_n^m \begin{Bmatrix}\cos m\lambda\\ \sin m\lambda\end{Bmatrix}$ vanish along (n-m) circles of latitude and also because of the factors cos $m\lambda$ or sin $m\lambda$ along $2m$ meridians at equal intervals π/m. These zero lines divide the surface of the sphere into regions in each of which the

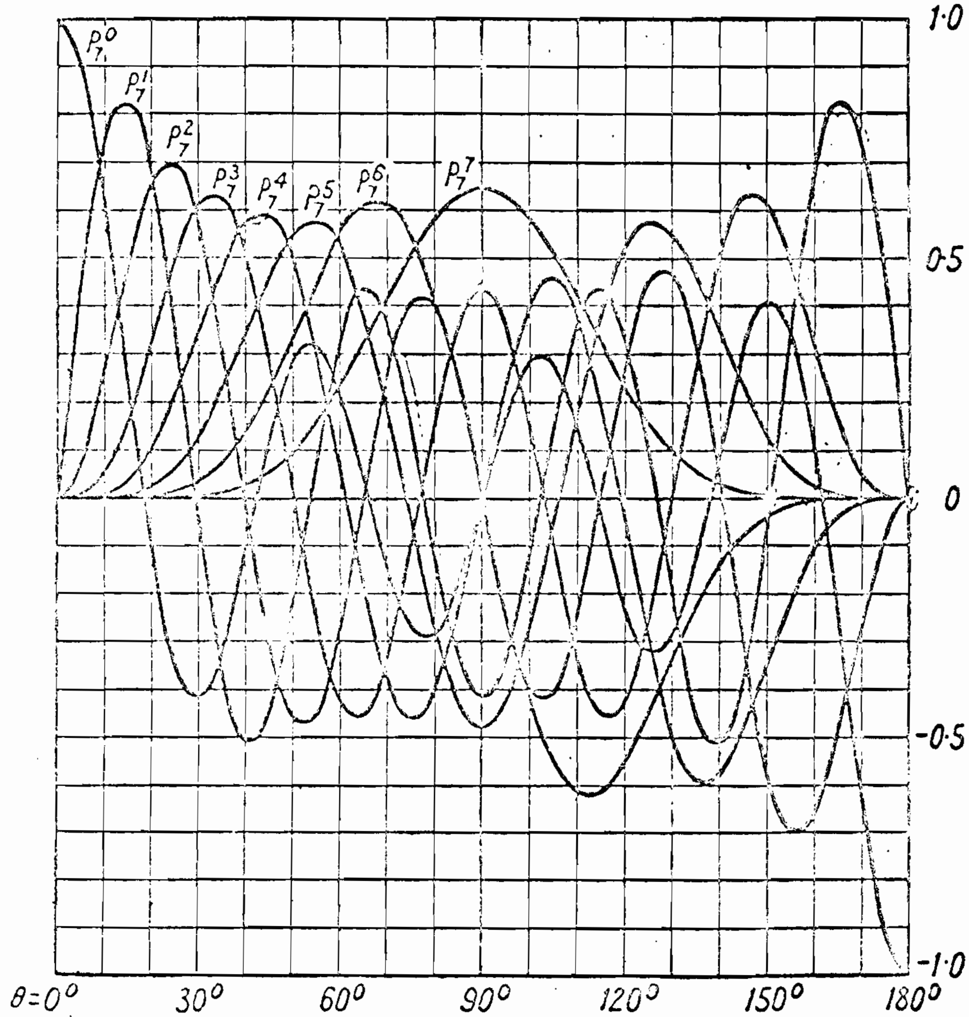

FIG. 13. The associated harmonics $P_7^0, P_7^1, \ldots, P_7^7$ as functions of θ.
(After Chapman and Bartels.)

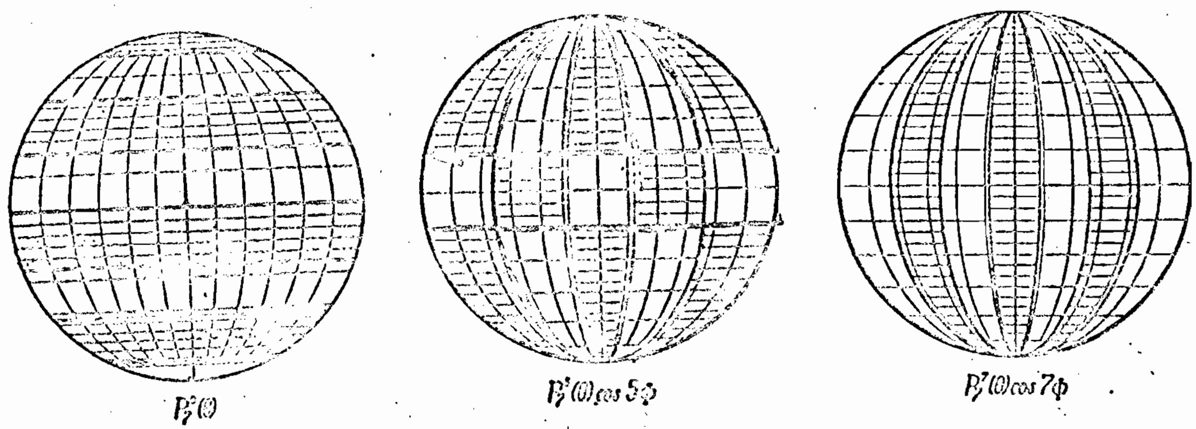

Figure 14. Equal area map of the zero-lines (thick lines in diagram), over one hemisphere, of a zonal harmonic (P_7^0), a tesseral harmonic ($P_7^5 \cos 7\lambda$); the central meridian corresponds to $\lambda = 0$. The areas in which the sign of the function is positive are indicated by drawing the (thin-line) circles of latitude at closer intervals.

sign of the surface harmonic is constant, while it is reversed on crossing the boundary between two adjacent regions. Consequently, for $n > m > 0$, the surface harmonics are called tesseral surface harmonics. When $m=0$, the functions are called zonal surface harmonics. When $m=n$, the functions are called sectorial surface harmonics, because there are no circles of latitude along which the functions vanishes; the regions of constant signs are therefore sectors of the sphere. Figure 14 shows this for $P_7^0(0)\cos O$, $P_7^5 \cos 5\lambda$ and $P_7^7 \cos 7\lambda$.

There are 2m+1 tesseral harmonics of the n^{th} degree. If each of these is multiplied by a constant and their sum is taken, this sum is called a Surface Harmonic of the n^{th} degree.

<u>$P_n^m(\theta)$ As a Solution of the Vorticity Equation</u>

$$\zeta = \frac{1}{a\sin\theta}\left[\frac{\partial}{\partial\theta}\left\{\sin\theta\,(u+V)\right\} - \frac{\partial V}{\partial\lambda}\right]$$

Conservation of vorticity yields,

$$\zeta + 2\omega\cos\theta = \text{constant}$$

Substituting the expression for ζ and differentiating with respect to time, we obtain

$$\left(\frac{\partial}{\partial t} - \alpha\frac{\partial}{\partial\lambda}\right)\left[\frac{1}{a\sin\theta}\left(\frac{\partial}{\partial\theta}(\sin\theta\,u) - \frac{\partial v}{\partial\lambda}\right)\right] + v\frac{\partial}{\partial\theta}\left[\frac{}{a\sin\theta}\frac{\partial}{\partial\theta}(\sin\theta\,V)\right] = \frac{2\omega\sin\theta\,v}{a}$$

Using the stream function ψ, the vorticity equation becomes,

$$\left(\frac{\partial}{\partial t} - \alpha\frac{\partial}{\partial\lambda}\right)\frac{1}{\sin\theta}\left[\frac{\partial}{\partial\theta}\left(\sin\theta\frac{\partial\psi}{\partial\theta}\right) - \frac{1}{\sin\theta}\frac{\partial^2\psi}{\partial\lambda^2}\right] + 2(\omega+\alpha)\frac{\partial\psi}{\partial\lambda} = 0 \quad (11)$$

this form of the vorticity equation assumes

(a) Friction is negligible

(b) Vertical velocity is negligible

(c) Perturbation velocities u, v are so small that their second and higher powers are negligible

(d) Density of the air parcel remains constant while in motion

(e) Density does not vary in the horizontal plane.

Assume as a solution $\psi(t, \lambda, \theta) = \cos(\beta t + m\lambda) f(\theta)$

Substituting this into (11), we obtain

$$\left(\frac{\partial}{\partial t} + \alpha \frac{\partial}{\partial \lambda}\right) \frac{1}{\sin\theta}\left[\frac{\partial}{\partial\theta} \sin\theta \frac{\partial}{\partial\theta}\left[\cos(\beta t + m\lambda) f(\theta)\right] + \frac{1}{\sin\theta}\frac{\partial^2}{\partial\lambda^2}\left[\cos(\beta t + m\lambda) f(\theta)\right]\right]$$

$$+ 2(\omega + \alpha)\frac{\partial}{\partial\lambda}\left[\cos(\beta t + m\lambda) f(\theta)\right] = 0$$

i.e.

$$\left(\frac{\partial}{\partial t} + \alpha \frac{\partial}{\partial \lambda}\right) \frac{1}{\sin\theta}\left[\frac{\partial}{\partial\theta} \sin\theta \cos(\beta t + m\lambda) f'(\theta) - \frac{1}{\sin\theta}\cos(\beta t + m\lambda) m^2 f(\theta)\right]$$

$$+ 2(\omega + \alpha) m \sin(\beta t + m\lambda) f(\theta) = 0$$

$$\therefore \frac{\alpha}{\sin\theta}\left[\frac{\partial}{\partial\theta} \sin\theta \sin(\beta t + m\lambda) f'(\theta)\, m - \frac{1}{\sin\theta} f(\theta) m^3\right]$$

$$+ \frac{1}{\sin\theta}\left[\frac{\partial}{\partial\theta} \sin\theta f'(\theta)\beta - \frac{1}{\sin\theta} f(\theta) m^2 \beta\right] + 2(\omega + \alpha) m f(\theta) = 0$$

$$\therefore \frac{m\alpha}{\sin\theta}\frac{\partial}{\partial\theta} \sin\theta f'(\theta) - \frac{m^3\alpha}{\sin^2\theta} f(\theta) + \frac{\beta}{\sin\theta}\frac{\partial}{\partial\theta}\sin\theta f'(\theta)$$

$$- \frac{m^2\beta}{\sin^2\theta} f(\theta) + 2(\omega + \alpha) m f(\theta) = 0$$

$$\therefore\ -\frac{m^2}{\sin^2\theta}(\beta+\alpha m)f(\theta)+\frac{1}{\sin\theta}\frac{\partial}{\partial\theta}\left[\sin\theta(\beta+\alpha m)f'(\theta)\right]$$

$$+\,2(\omega+\alpha)mf(\theta)=0$$

$$\therefore\ \frac{1}{\sin\theta}\frac{\partial}{\partial\theta}\left(\sin\theta\frac{\partial f}{\partial\theta}\right)-\frac{m^2}{\sin^2\theta}f(\theta)+\frac{2(\omega+\alpha)m}{\beta+\alpha m}f(\theta)=0$$

$$\therefore\ \frac{1}{\sin\theta}\frac{d}{d\theta}\left(\sin\theta\frac{df}{d\theta}\right)+\left(\frac{2(\omega+\alpha)m}{\beta+\alpha m}-\frac{m^2}{\sin^2\theta}\right)f(\theta)=0 \qquad (12)$$

For equation (12) to be the Associated Legendre Differential Equation, we must have

$$\frac{2(\omega+\alpha)m}{\beta+\alpha m}=n(n+1) \qquad (13)$$

Hence $\quad f=C\,P_n^m(\cos\theta)$

and $\quad \psi=C\cos(\beta t+m\lambda)P_n^m(\cos\theta)$

From (13), the Rossby-Haurwitz angular phase velocity is found to be

$$\gamma=\alpha-\frac{2(\omega+\alpha)}{n(n+1)}$$